

**$\mu$  and  $\tau$  neutrino thermalization and production in supernovae: Processes and time scales**

Todd A. Thompson\*

*Department of Physics, The University of Arizona, Tucson, Arizona 85721*Adam Burrows<sup>†</sup>*Steward Observatory and Department of Astronomy, The University of Arizona, Tucson, Arizona 85721*Jorge E. Horvath<sup>‡</sup>*Instituto Astronômico e Geofísico, Universidade de São Paulo, Av. M. Stéfano 4200, Agua Funda, 04301-904, São Paulo, Brazil*

(Received 3 March 2000; published 11 August 2000)

We investigate the rates of production and thermalization of  $\nu_\mu$  and  $\nu_\tau$  neutrinos at temperatures and densities relevant to core-collapse supernovae and protoneutron stars. Included are contributions from electron scattering, electron-positron annihilation, nucleon-nucleon bremsstrahlung, and nucleon scattering. For the scattering processes, in order to incorporate the full scattering kinematics at arbitrary degeneracy, the structure function formalism developed by Reddy, Prakash, and Lattimer [Phys. Rev. D **58**, 013009 (1998)] and Burrows and Sawyer [Phys. Rev. C **58**, 554 (1998)] is employed. Furthermore, we derive formulas for the total and differential rates of nucleon-nucleon bremsstrahlung for arbitrary nucleon degeneracy in asymmetric matter. We find that electron scattering dominates nucleon scattering as a thermalization process at low neutrino energies ( $\varepsilon_\nu \lesssim 10$  MeV), but that nucleon scattering is always faster than or comparable to electron scattering above  $\varepsilon_\nu \approx 10$  MeV. In addition, for  $\rho \gtrsim 10^{13}$  g cm<sup>-3</sup>,  $T \lesssim 14$  MeV, and neutrino energies  $\lesssim 60$  MeV, nucleon-nucleon bremsstrahlung always dominates electron-positron annihilation as a production mechanism for  $\nu_\mu$  and  $\nu_\tau$  neutrinos.

PACS number(s): 25.30.Pt, 26.50.+x, 13.15.+g, 97.60.Bw

**I. INTRODUCTION**

The cores of protoneutron stars and core-collapse supernovae are characterized by mass densities of order  $\sim 10^{10}$ – $10^{14}$  g cm<sup>-3</sup> and temperatures that range from  $\sim 1$  to 50 MeV. The matter is composed predominantly of nucleons, electrons, positrons, and neutrinos of all species. For  $\nu_\mu$  and  $\nu_\tau$  types (collectively  $\nu_\mu$ 's), which carry away 50–60% of the  $\sim 2$ – $3 \times 10^{53}$  ergs liberated during collapse and explosion, the prevailing opacity and production processes are  $\nu_\mu$ -electron scattering,  $\nu_\mu$ -nucleon scattering, electron-positron annihilation ( $e^+e^- \leftrightarrow \nu_\mu \bar{\nu}_\mu$ ), and nucleon-nucleon bremsstrahlung. While all of these processes contribute for the electron types ( $\nu_e$ 's and  $\bar{\nu}_e$ 's), the charged-current absorption processes  $\nu_e n \leftrightarrow p e^-$  and  $\bar{\nu}_e p \leftrightarrow n e^+$  dominate their opacity so completely that in this paper we address only  $\nu_\mu$  production and thermalization.

Supernova theorists had long held [1] that  $\nu_\mu$ -nucleon scattering was unimportant as a mechanism for neutrino equilibration. While this process was included as a source of opacity [2,3], it served only to redistribute the neutrinos in space, not in energy. In contrast,  $\nu_\mu$ -electron scattering was thought to dominate  $\nu_\mu$  neutrino thermalization. In addition, the only  $\nu_\mu \bar{\nu}_\mu$  pair production mechanisms employed in full supernova calculations were  $e^+e^- \leftrightarrow \nu_\mu \bar{\nu}_\mu$  and plasmon de-

cay ( $\gamma_{pl} \leftrightarrow \nu_\mu \bar{\nu}_\mu$ ) [2]; nucleon-nucleon bremsstrahlung was neglected as a source. Recent developments, however, call both these practices into question and motivate a reevaluation of these opacities in the supernova context. Analytic formulas have recently been derived [4–6] which include the full nucleon kinematics and Pauli blocking in the final state at arbitrary nucleon degeneracy. These efforts reveal that the average rate of energy transfer in  $\nu_\mu$ -nucleon scattering may surpass previous estimates by an order of magnitude [5,7–11]. Hence, this process may compete with  $\nu_\mu$ -electron scattering as an equilibration mechanism. Similarly, estimates for the total nucleon-nucleon bremsstrahlung rate have been obtained [7,12–14] which indicate that this process might compete with  $e^+e^-$  annihilation.

These results suggest that the time is ripe for a technical study of the relative importance of each process for production or thermalization. To conduct such a study, we consider  $\nu_\mu$  neutrinos in an isotropic homogeneous thermal bath of scatterers and absorbers. In this system, the full transport problem is reduced to an evolution of the neutrino distribution function ( $\mathcal{F}_\nu$ ) in energy space alone. Although this is a simplification of the true problem, it provides a theoretical laboratory in which to analyze the rates both for equilibration of an initial neutrino distribution function with dense nuclear matter and for production of the neutrinos themselves. From these rates we determine the importance and particular character of each process, and discover in which energy, temperature, or density regime each dominates. We employ a general prescription for solving the Boltzmann equation in this system with the full energy redistribution collision term. We compare quantitatively, via direct numerical evolution of

\*Electronic address: thomp@physics.arizona.edu

†Electronic address: burrows@jupiter.as.arizona.edu

‡Electronic address: foton@orion.iagusp.usp.br

an arbitrary neutrino distribution function, the rates for thermalization and production by each process, at all neutrino energies. Furthermore, we present the total nucleon-nucleon bremsstrahlung rate for arbitrary nucleon degeneracy and derive the single  $\nu_\mu$  and  $\bar{\nu}_\mu$  production spectra. This facilitates a more comprehensive evaluation of its relative importance in neutrino production than has previously been possible.

In Sec. II, we discuss the general form of the Boltzmann equation and our use of it to study  $\nu_\mu$  equilibration and production rates. In Sec. III, we provide formulas for each of the four processes we consider:  $\nu_\mu$ -nucleon scattering,  $\nu_\mu$ -electron scattering, and  $\nu_\mu\bar{\nu}_\mu$  pair production via both nucleon-nucleon bremsstrahlung and  $e^+e^-$  annihilation. In Sec. IV, we present the results of our equilibration calculations, showing the time evolution of  $\nu_\mu$  distribution functions as influenced by each of these processes individually. We include plots of thermalization and production rates for each process as a function of neutrino energy and time. For the scattering interactions we include figures of the time evolution of the net energy transfer to the medium as a function of incident neutrino energy. We repeat this analysis at points in temperature, density, and composition space relevant to supernovae and proton-neutron stars, taken from snapshots of a stellar profile during a realistic collapse calculation [3]. Using these results, we discuss the relative importance of each process in shaping the emergent  $\nu_\mu$  spectrum. In Sec. V, we recapitulate our findings and conclusions.

## II. THE BOLTZMANN EQUATION

The static (velocity=0) Boltzmann equation for the evolution of the neutrino distribution function ( $\mathcal{F}_\nu$ ), including Pauli blocking in the final state, and for a spherical geometry, is

$$\left( \frac{1}{c} \frac{\partial}{\partial t} + \mu \frac{\partial}{\partial r} + \frac{1-\mu^2}{r} \frac{\partial}{\partial \mu} \right) \mathcal{F}_\nu = (1-\mathcal{F}_\nu)j_\nu - \mathcal{F}_\nu\chi_\nu, \quad (1)$$

where  $t$  is the time,  $r$  is the radial coordinate, and  $\mu$  ( $=\cos\theta$ ) is the cosine of the zenith angle.  $j_\nu$  and  $\chi_\nu$  are the total *source* and *sink*, respectively. For emission and absorption,  $j_\nu$  is the emissivity and  $\chi_\nu$  is the extinction coefficient. For scattering, both  $j_\nu$  and  $\chi_\nu$  are energy redistribution integrals which couple one neutrino energy bin with all the others. The matrix element and associated phase-space integrations that comprise  $j_\nu$  and  $\chi_\nu$  for electron and nucleon scattering yield the probability that a given collision will scatter a particle into any angle or energy bin. A full transport calculation couples energy and angular bins to each other through the right hand side of Eq. (1).

In a homogeneous, isotropic thermal bath of scatterers and absorbers no spatial or angular gradients exist. Consequently, the Boltzmann equation becomes

$$\frac{1}{c} \frac{\partial \mathcal{F}_\nu}{\partial t} = (1-\mathcal{F}_\nu)j_\nu - \mathcal{F}_\nu\chi_\nu. \quad (2)$$

By dealing with this system, the transport problem reduces to an evolution of  $\mathcal{F}_\nu$  in just energy and time. Note that for

scattering processes, both  $j_\nu$  and  $\chi_\nu$  require an integral over the scattered neutrino distribution function  $\mathcal{F}'_\nu$ . Similarly, in evolving  $\mathcal{F}_\nu$  via the production and absorption processes,  $j_\nu$  and  $\chi_\nu$  involve an integration over the antineutrino distribution function  $\mathcal{F}'_{\bar{\nu}}$ . Therefore,  $\mathcal{F}'_{\bar{\nu}}$  must be evolved simultaneously with  $\mathcal{F}_\nu$ . While  $j_\nu$  and  $\chi_\nu$  may be fairly complicated integrals over phase space, the numerical solution of Eq. (2) is straightforward.

Given an arbitrary initial  $\mathcal{F}_\nu$ , we divide the relevant energy range into  $n$  energy bins. We then solve Eq. (2) for each bin individually and explicitly. Angular integrals over scattering cosines, which appear in the  $\nu_\mu$ -nucleon and  $\nu_\mu$ -electron scattering formalism, as well as the electron energy integration needed for  $e^+e^-$  annihilation, are carried out with a four-point Gauss-Legendre integration scheme. The double integral over dimensionless nucleon momentum variables needed to obtain the contribution from nucleon-nucleon bremsstrahlung is computed using nested 16-point Gauss-Laguerre quadratures.

### Rates for $\mathcal{F}_\nu$ evolution and energy transfer

Scattering, emission, and absorption processes, at a given neutrino energy  $\varepsilon_\nu$ , produce and remove neutrinos from the phase-space density at that energy. The former achieves this by transferring energy to the matter during scattering, the latter two by emitting or absorbing directly from that bin. The Boltzmann equation can then be written in terms of an in and an out channel, the former a source and the latter a sink

$$\frac{\partial \mathcal{F}_\nu}{\partial t} = \frac{\partial \mathcal{F}_\nu}{\partial t} \Big|_{\text{in}} - \frac{\partial \mathcal{F}_\nu}{\partial t} \Big|_{\text{out}}. \quad (3)$$

Consequently, for any interaction, there are two rates to consider: the rate for scattering or production into a given energy bin  $\Gamma_{\text{in}}$  and the inverse rate for scattering or absorption out of that bin  $\Gamma_{\text{out}}$ . The rates  $cj_\nu$  and  $c\chi_\nu$  yield time scales for an interaction to occur, but fail, in the case of the former, to fold in Pauli blocking in the final state. Equation (3) includes these effects and provides natural time scales for  $\mathcal{F}_\nu$  evolution

$$\Gamma_{\text{in}} = \frac{1}{\mathcal{F}_\nu} \frac{\partial \mathcal{F}_\nu}{\partial t} \Big|_{\text{in}} = \frac{(1-\mathcal{F}_\nu)}{\mathcal{F}_\nu} cj_\nu, \quad (4)$$

and

$$\Gamma_{\text{out}} = \frac{1}{\mathcal{F}_\nu} \frac{\partial \mathcal{F}_\nu}{\partial t} \Big|_{\text{out}} = c\chi_\nu. \quad (5)$$

Note that although Eq. (5) does not explicitly contain a Pauli blocking term,  $\chi_\nu$  contains an integral over  $(1-\mathcal{F}'_\nu)$ , in the case of scattering, and an appropriate final-state blocking term, in the case of absorption. At a given  $\varepsilon_\nu$ , then,  $\Gamma_{\text{in}}$  incorporates information about the  $\nu_\mu$  phase-space density at that energy. Conversely, at that same  $\varepsilon_\nu$ ,  $\Gamma_{\text{out}}$  contains information about the phase space at all other energies. Regardless of the initial distribution,  $\partial \mathcal{F}_\nu / \partial t = 0$  in equilibrium.

This implies  $\Gamma_{\text{in}} = \Gamma_{\text{out}}$  in equilibrium and, hence, we build in a test for the degree to which the system has thermalized.

Just as there are distinct rates for the in and out channels of the Boltzmann equation during equilibration, so too are there distinct scattering energy transfers. For  $\nu_\mu$  scattering with a scatterer  $s$  (electron or nucleon), at a specific  $\varepsilon_\nu$ , two thermal average energy transfers can be defined

$$\langle \omega \rangle_{\text{in}} = \int d^3 p'_\nu \omega \mathcal{F}'_\nu \mathcal{I}^{\text{in}}[\nu_\mu s \leftarrow \nu'_\mu s'] / \int d^3 p'_\nu \mathcal{F}'_\nu \times \mathcal{I}^{\text{in}}[\nu_\mu s \leftarrow \nu'_\mu s'] \quad (6)$$

and

$$\langle \omega \rangle_{\text{out}} = \int d^3 p'_\nu \omega (1 - \mathcal{F}'_\nu) \mathcal{I}^{\text{out}}[\nu_\mu s \rightarrow \nu'_\mu s'] / \int d^3 p'_\nu \times (1 - \mathcal{F}'_\nu) \mathcal{I}^{\text{out}}[\nu_\mu s \rightarrow \nu'_\mu s'], \quad (7)$$

where primes denote the scattered neutrino,  $\omega (= \varepsilon_\nu - \varepsilon'_\nu)$  is the energy transfer, and  $\mathcal{I}^{\text{in}}$  and  $\mathcal{I}^{\text{out}}$  are the kernels for scattering into and out of a given energy bin, respectively. As a consequence of detailed balance between the in and out channels of the Boltzmann equation,  $\mathcal{I}^{\text{in}} = e^{-\beta\omega} \mathcal{I}^{\text{out}}$ , where  $\beta = 1/k_B T$  and  $T$  is the matter temperature. (The scattering kernels are discussed in detail in Sec. III for both scattering processes.) Note that the denominators in Eqs. (6) and (7), up to constants that divide out in the definitions of  $\langle \omega \rangle_{\text{in}}$  and  $\langle \omega \rangle_{\text{out}}$ , are just  $j_\nu$  and  $\chi_\nu$ , respectively.

In an effort to provide more than one measure of the time scale for  $\mathcal{F}_\nu$  equilibration due to scattering and to make contact with previous neutrino thermalization studies [15–17] we also define a set of time scales in terms of  $\langle \omega \rangle_{\text{out}}$  and the higher  $\omega$  moment,  $\langle \omega^2 \rangle_{\text{out}}$

$$\Gamma_D = c \chi_\nu \left| \frac{\langle \omega \rangle_{\text{out}}}{\varepsilon_\nu} \right| \quad (8)$$

and

$$\Gamma_E = c \chi_\nu \frac{\langle \omega^2 \rangle_{\text{out}}}{\varepsilon_\nu^2}. \quad (9)$$

$\Gamma_D$  is the rate for shifting the centroid of a given distribution and  $\Gamma_E$  is the rate for spreading an initial distribution [15]. In contrast with the work of Refs. [15–17], we include the full effects of Pauli blocking in the final state, allowing us to deal consistently with cases in which the  $\nu_\mu$ 's are partially degenerate.

### III. INDIVIDUAL INTERACTIONS

This section details the source and sink terms necessary to solve the Boltzmann equation for the time evolution of  $\mathcal{F}_\nu$ . Sections III A and III B are dedicated to the presentation and discussion of the collision terms for  $\nu_\mu$ -nucleon and  $\nu_\mu$ -electron scattering, respectively. Section III C describes the Legendre series expansion approximation and the use of it to compute the contribution to the Boltzmann equation, the

pair emissivity, and the single  $\nu_\mu$  spectrum due to  $e^+ e^- \leftrightarrow \nu_\mu \bar{\nu}_\mu$ . Our derivations of  $j_\nu$  and  $\chi_\nu$ , as well as the single and pair spectra from nucleon-nucleon bremsstrahlung at arbitrary nucleon degeneracy and in the nondegenerate limit, are presented in Sec. III D. In what follows, we take  $G^2 \simeq 1.55 \times 10^{-33} \text{ cm}^3 \text{ MeV}^{-2} \text{ s}^{-1}$ ,  $\sin^2 \theta_W \simeq 0.231$ , and employ natural units in which  $\hbar = c = k_B = 1$ .

#### A. Nucleon scattering: $\nu_\mu n \leftrightarrow \nu_\mu n$ and $\nu_\mu p \leftrightarrow \nu_\mu p$

Researchers working on supernova and protoneutron star evolution have recently reevaluated the issue of energy transfer via  $\nu_\mu$ -nucleon scattering [5,7–10]. Originally, the assumption was made that the nucleons were stationary [1]. If a neutron of mass  $m_n$  is at rest with respect to an incoming neutrino of energy  $\varepsilon_\nu$ , one finds that the energy transfer ( $\bar{\omega}$ ) is  $\sim -\varepsilon_\nu^2/m_n$ . For  $\varepsilon_\nu = 10 \text{ MeV}$ ,  $\bar{\omega} \sim -0.1 \text{ MeV}$ , a fractional energy lost of 1%. Using these simple kinematic arguments and disregarding neutrino and nucleon Pauli blocking, one finds that the thermalization rate for  $\nu_\mu$ -electron scattering should be approximately a factor of 20 larger than that for  $\nu_\mu$ -nucleon scattering. In the context of interest, however, at temperatures of order 10 MeV and mass densities of order  $10^{13} \text{ g cm}^{-3}$ , free nucleons are not stationary, but have thermal velocities. The fractional energy exchange per collision, in the case of  $\nu_\mu$ -neutron scattering, is then  $\sim p_n/m_n c$  [5]. For  $T \sim 10 \text{ MeV}$  this gives a  $\sim 10\% - 20\%$  change in  $\varepsilon_\nu$  per collision. This calls the naive estimate of the relative importance of  $\nu_\mu$ -nucleon scattering as a thermalization process into question and a more complete exploration of the relative importance of the two scattering processes is necessary.

Recently, analytic formulas have been derived which include the full kinematics of  $\nu_\mu$ -nucleon scattering at arbitrary nucleon degeneracy [4–6]. At the temperatures and densities encountered in the supernova context noninteracting nucleons are not relativistic. Due to nucleon-nucleon interactions, however, at and around nuclear density ( $\sim 2.68 \times 10^{14} \text{ g cm}^{-3}$ ), the nucleon's effective mass drops and is expected to be comparable with its Fermi momentum [4]. In such a circumstance, a relativistic description of the  $\nu_\mu$ -nucleon scattering interaction is warranted. In addition, spin and density correlation effects engendered by these nucleon-nucleon interactions have been found to suppress the  $\nu_\mu$ -nucleon interaction rate by as much as a factor of  $\sim 2-3$  [5,10,11].

In this study, we focus on  $\nu_\mu$  equilibration rates at densities  $\lesssim 1 \times 10^{14} \text{ g cm}^{-3}$  where it is still unclear if nucleon-nucleon interactions will play an important role. This ambiguity is due in part to uncertainties both in the nuclear equation of state and the nucleon-nucleon interaction itself. For this reason, in considering neutrino-nucleon scattering, we choose to treat the nucleons as nonrelativistic and noninteracting, thereby ignoring collective effects which might enhance or reduce the  $\nu_\mu$ -nucleon scattering rate. Particularly, in calculating this scattering rate, we ignore the effect of inelastic nucleon-nucleon scattering (e.g.,  $\nu_\mu nn \leftrightarrow \nu_\mu nn$ ) [7]. Making these assumptions, we find that  $j_\nu$  and  $\chi_\nu$  in Eq. (2) are given by

$$j_\nu = \frac{G^2}{(2\pi)^3} \int d^3\vec{p}'_\nu \mathcal{I}_{\text{NC}} \mathcal{F}'_\nu e^{-\beta\omega} \quad (10)$$

and

$$\chi_\nu = \frac{G^2}{(2\pi)^3} \int d^3\vec{p}'_\nu \mathcal{I}_{\text{NC}} [1 - \mathcal{F}'_\nu], \quad (11)$$

where  $\beta = 1/T$ ,  $\vec{p}'_\nu$  is the final state neutrino momentum, and  $\omega$  is the energy transfer. In Eqs. (10) and (11), the neutral-current scattering kernel is given by

$$\mathcal{I}_{\text{NC}} = S(q, \omega) [(1 + \mu)V^2 + (3 - \mu)A^2], \quad (12)$$

where  $\mu (= \cos \theta)$  is the cosine of the scattering angle between incident and final state neutrinos and  $S(q, \omega)$  is the dynamic structure function. In Eq. (12),  $V$  and  $A$  are the appropriate vector and axial-vector coupling constants; for  $\nu_\mu$ -neutron scattering,  $V = -1/2$  and  $A = -1.26/2$ . The dynamic structure function is

$$\begin{aligned} S(q, \omega) &= 2 \int \frac{d^3\vec{p}}{(2\pi)^3} \mathcal{F}(1 - \mathcal{F}') (2\pi) \delta(\omega + \varepsilon - \varepsilon') \\ &= 2 \text{Im} \Pi^{(0)}(q, \omega) (1 - e^{-\beta\omega})^{-1}, \end{aligned} \quad (13)$$

where  $q = |p_\nu - p'_\nu| = [\varepsilon_\nu^2 + \varepsilon_\nu'^2 - 2\varepsilon_\nu \varepsilon'_\nu \mu]^{1/2}$  is the magnitude of the momentum transfer, and  $\mathcal{F}$  and  $\mathcal{F}'$  are the incident and scattered nucleon distribution functions, respectively. In Eq. (13),  $\vec{p}$  is the incident nucleon momentum,  $\varepsilon$  is the incident nucleon energy, and  $\varepsilon'$  is the scattered nucleon energy. The imaginary part of the free polarization is given by [5,18]

$$\text{Im} \Pi^{(0)}(q, \omega) = \frac{m^2}{2\pi\beta q} \ln \left[ \frac{1 + e^{-Q^2 + \eta}}{1 + e^{-Q^2 + \eta - \beta\omega}} \right], \quad (14)$$

where

$$Q = \left( \frac{m\beta}{2} \right)^{1/2} \left( -\frac{\omega}{q} + \frac{q}{2m} \right), \quad (15)$$

$\eta$  is the nucleon degeneracy ( $\mu/T$ ), and  $m$  is the nucleon mass. The factor  $e^{-\beta\omega}$  that appears in Eq. (10) is a consequence of the fact that  $S(q, -\omega) = e^{-\beta\omega} S(q, \omega)$ , itself a consequence of detailed balance between the in and out channels of the Boltzmann equation. The dynamic structure function can be thought of as a correlation function that connects  $\varepsilon_\nu$  and  $\varepsilon'_\nu$ .

The  $\phi$  angular integrations implicit in Eqs. (10) and (11) can be computed trivially assuming the isotropy of  $\mathcal{F}_\nu$ . Furthermore, by defining the coordinate system with the momentum vector of the incident neutrino, the scattering angle and the direction cosine are equivalent. Combining these two equations in the Boltzmann equation for the evolution of  $\mathcal{F}_\nu$  due to neutral-current  $\nu_\mu$ -nucleon scattering, we obtain

$$\begin{aligned} \frac{\partial \mathcal{F}_\nu}{\partial t} &= \frac{G^2}{(2\pi)^2} \int_0^\infty d\varepsilon'_\nu \varepsilon_\nu'^2 \int_{-1}^1 d\mu \mathcal{I}_{\text{NC}} \\ &\times \{ [1 - \mathcal{F}_\nu] \mathcal{F}'_\nu e^{-\beta\omega} - \mathcal{F}_\nu [1 - \mathcal{F}'_\nu] \}. \end{aligned} \quad (16)$$

### B. Electron scattering: $\nu_\mu e^- \leftrightarrow \nu_\mu e^-$

At the temperatures and densities encountered in supernovae and protoneutron stars, electrons are highly relativistic. A formalism analogous to that used for  $\nu_\mu$ -nucleon scattering is desired in order to include the full electron kinematics at arbitrary electron degeneracy. Reddy, Prakash, and Lattimer [4] have developed a relativistic generalization of the structure function formalism described in Sec. III A. They obtain a set of polarization functions which characterize the relativistic medium's response to a neutrino probe in terms of polylogarithmic functions. In analogy with Eq. (16), we can write the Boltzmann equation for the evolution of  $\mathcal{F}_\nu$  due to  $\nu_\mu$ -electron scattering as

$$\frac{\partial \mathcal{F}_\nu}{\partial t} = \frac{G^2}{(4\pi)^3} \int d^3p'_\nu \mathcal{I}'_{\text{NC}} \{ [1 - \mathcal{F}_\nu] \mathcal{F}'_\nu e^{-\beta\omega} - \mathcal{F}_\nu [1 - \mathcal{F}'_\nu] \}, \quad (17)$$

where  $\mathcal{I}'_{\text{NC}}$  is the relativistic neutral-current scattering kernel for  $\nu_\mu$ 's, analogous to  $\mathcal{I}_{\text{NC}}$  in Eq. (12). All the physics of the interaction is contained in  $\mathcal{I}'_{\text{NC}}$ , which can be written as

$$\mathcal{I}'_{\text{NC}} = \frac{q_\mu^2}{\varepsilon_\nu \varepsilon'_\nu} \text{Im} \{ \Lambda^{\alpha\beta} \Pi_{\alpha\beta}^R \} (1 - e^{-\beta\omega})^{-1}, \quad (18)$$

where  $q_\mu (= (\omega, \vec{q}))$  is the four-momentum transfer. As in the nonrelativistic case,  $\mathcal{I}'_{\text{NC}}$  is composed of the lepton tensor

$$\Lambda^{\alpha\beta} = 8 [2k^\alpha k^\beta + (k \cdot q) g^{\alpha\beta} - (k^\alpha q^\beta + q^\alpha k^\beta) - i \varepsilon^{\alpha\beta\mu\nu} k^\mu q^\nu], \quad (19)$$

which is just the squared and spin-summed matrix element for the scattering process written in terms of  $k_\alpha$ , the incident  $\nu_\mu$  four-momentum. The scattering kernel also contains the retarded polarization tensor,  $\Pi_{\alpha\beta}^R$ , which is directly analogous to the free polarization in the nonrelativistic case given in Eq. (13). The retarded polarization tensor is related to the causal polarization by

$$\text{Im} \Pi_{\alpha\beta}^R = \tanh(-\frac{1}{2}\beta\omega) \text{Im} \Pi_{\alpha\beta} \quad (20)$$

and

$$\Pi_{\alpha\beta} = -i \int \frac{d^4p}{(2\pi)^4} \text{Tr} [G_e(p) J_\alpha G_e'(p+q) J_\beta]. \quad (21)$$

In Eq. (21),  $p_\alpha$  is the electron four momentum and  $J_\alpha$  is the current operator. The electron Green's functions ( $G_e$  and  $G_e'$ ), explicit in the free polarization, connect points in electron energy space and characterize the effect of the interac-

tion on relativistic electrons. The polarization tensor can be written in terms of a vector part, an axial-vector part, and a mixed part, so that

$$\Pi_{\alpha\beta} = V^2 \Pi_{\alpha\beta}^V + A^2 \Pi_{\alpha\beta}^A - 2VA \Pi_{\alpha\beta}^{VA}. \quad (22)$$

In turn, the vector part of the polarization tensor can be written in terms of two independent components:  $\Pi_T$  and  $\Pi_L$ . In contrast with Eq. (12), since  $v/c \sim 1$  for the electrons, the angular terms which were dropped from the matrix element in the nonrelativistic case, leading to a single structure function, must now be retained.  $\mathcal{I}_{\text{NC}}^r$  can then be written as a set of three structure functions [4]

$$\begin{aligned} \mathcal{I}_{\text{NC}}^r = & 8 \frac{q_\mu^2}{\varepsilon_\nu \varepsilon'_\nu} [A \mathcal{S}_1(q, \omega) + \mathcal{S}_2(q, \omega) \\ & + B \mathcal{S}_3(q, \omega)] (1 - e^{-\beta\omega})^{-1}, \end{aligned} \quad (23)$$

where  $A = (4\varepsilon_\nu \varepsilon'_\nu + q_\alpha^2)/2q^2$  and  $B = \varepsilon_\nu + \varepsilon'_\nu$ . These structure functions can be written in terms of the vector parts of the retarded polarization tensor ( $\Pi_T^R$  and  $\Pi_L^R$ ), the axial part ( $\Pi_A^R$ ), and the mixed part ( $\Pi_{VA}^R$ )

$$\mathcal{S}_1(q, \omega) = (V^2 + A^2) [\text{Im} \Pi_L^R(q, \omega) + \text{Im} \Pi_T^R(q, \omega)], \quad (24)$$

$$\mathcal{S}_2(q, \omega) = (V^2 + A^2) \text{Im} \Pi_T^R(q, \omega) - A^2 \text{Im} \Pi_A^R(q, \omega), \quad (25)$$

and

$$\mathcal{S}_3(q, \omega) = 2VA \text{Im} \Pi_{VA}^R(q, \omega). \quad (26)$$

The retarded polarization functions, in terms of differences between polylogarithmic integrals, can be found in Appendix A.

### C. Electron-positron annihilation: $e^+ e^- \leftrightarrow \nu_\mu \bar{\nu}_\mu$

Fermi's Golden Rule for the total volumetric emission rate for the production of  $\nu_\mu$ 's via electron-positron annihilation can be written as

$$\begin{aligned} Q = & \int \frac{d^3 \vec{p}}{(2\pi)^3 2\varepsilon} \frac{d^3 \vec{p}'}{(2\pi)^3 2\varepsilon'} \frac{d^3 \vec{q}_\nu}{(2\pi)^3 2\varepsilon_\nu} \frac{d^3 \vec{q}_{\bar{\nu}}}{(2\pi)^3 2\varepsilon_{\bar{\nu}}} \varepsilon_\nu \\ & \times \left( \frac{1}{4} \sum_s |\mathcal{M}^2| \right) (2\pi)^4 \delta^4(P) \Xi[\mathcal{F}], \end{aligned} \quad (27)$$

where

$$\Xi[\mathcal{F}] = (1 - \mathcal{F}_\nu)(1 - \mathcal{F}_{\bar{\nu}}) \mathcal{F}_e - \mathcal{F}_{e^+}, \quad (28)$$

and  $\delta^4(P)$  conserves the four momentum.  $\mathcal{F}_{e^-}$  and  $\mathcal{F}_{e^+}$  are the electron and positron distribution functions. In Eq. (27),  $p_\alpha (= (\varepsilon, \vec{p}))$  and  $p'_\alpha (= (\varepsilon', \vec{p}'))$  are the four-momenta of the electron and positron, respectively, and  $q_\nu^\alpha (= (\varepsilon_\nu, \vec{q}_\nu))$  and  $q_{\bar{\nu}}^\alpha (= (\varepsilon_{\bar{\nu}}, \vec{q}_{\bar{\nu}}))$  are the four-momenta of the  $\nu_\mu$  and  $\bar{\nu}_\mu$ , respectively. The process of electron-positron annihilation into

a neutrino/anti-neutrino pair is related to neutrino-electron scattering considered in Sec. III B via a crossing symmetry. In order to make the problem tractable, we follow the standard procedure [2] of expanding the production kernel in a Legendre series in the scattering angle to first order (see Appendix B). Near the neutrino spheres, at densities which render neutrino transport diffusive, this approximation holds. In a full neutrino transport algorithm, however, which must handle both the diffusion and free-streaming limits, the second-order term, with proper closure relations, must be used in the semitransparent regime between the neutrino spheres and the shock [19]. Having made this approximation, including only the zeroth- and first-order terms, the single  $\nu_\mu$  spectrum is

$$\frac{dQ}{d\varepsilon_\nu} = (1 - \mathcal{F}_\nu) \frac{\varepsilon_\nu^3}{8\pi^4} \int_0^\infty d\varepsilon_{\bar{\nu}} \varepsilon_{\bar{\nu}}^2 \Phi_0^p(\varepsilon_\nu, \varepsilon_{\bar{\nu}}) (1 - \mathcal{F}_{\bar{\nu}}), \quad (29)$$

where  $\Phi_0^p(\varepsilon_\nu, \varepsilon_{\bar{\nu}})$  is the zeroth-order production kernel expansion coefficient, an integral over the electron energy (see Appendix B) [2]. With the differential spectrum or emissivity ( $dQ/d\varepsilon_\nu$ ) in hand, it is a simple matter to extract the contribution to the Boltzmann equation due to  $e^+ e^-$  annihilation. As Eq. (29) already contains the  $\nu_\mu$  blocking factor, the contribution to the Boltzmann equation, the in channel explicit in Eq. (3) can be written as [2]

$$\left. \frac{\partial \mathcal{F}_\nu}{\partial t} \right|_{\text{in}} = \frac{1}{4\pi} \frac{(2\pi)^3}{\varepsilon_\nu^3} \frac{dQ}{d\varepsilon_\nu}. \quad (30)$$

In order to obtain the out channel for absorption due to  $e^+ e^-$  annihilation, we need only replace  $\mathcal{F}_e - \mathcal{F}_{e^+}$  in Eq. (28) with an electron/positron blocking term,  $(1 - \mathcal{F}_{e^-})(1 - \mathcal{F}_{e^+})$ , and replace the  $\nu_\mu$  and  $\bar{\nu}_\mu$  blocking terms in Eq. (29) with  $\mathcal{F}_\nu \mathcal{F}_{\bar{\nu}}$ . Finally, the Boltzmann equation for the evolution of  $\mathcal{F}_\nu$  in time due to  $e^+ e^- \leftrightarrow \nu_\mu \bar{\nu}_\mu$  can be written as

$$\begin{aligned} \frac{\partial \mathcal{F}_\nu}{\partial t} = & \frac{2G^2}{(2\pi)^3} \int_0^\infty d\varepsilon_{\bar{\nu}} \varepsilon_{\bar{\nu}}^2 \int_0^\epsilon d\varepsilon H_0(\varepsilon_\nu, \varepsilon_{\bar{\nu}}, \varepsilon) \\ & \times \{ (1 - \mathcal{F}_\nu)(1 - \mathcal{F}_{\bar{\nu}}) \mathcal{F}_e - \mathcal{F}_{e^+} - \mathcal{F}_\nu \mathcal{F}_{\bar{\nu}} \\ & \times (1 - \mathcal{F}_{e^-})(1 - \mathcal{F}_{e^+}) \}, \end{aligned} \quad (31)$$

where  $\epsilon = \varepsilon_\nu + \varepsilon_{\bar{\nu}}$  and  $H_0(\varepsilon_\nu, \varepsilon_{\bar{\nu}}, \varepsilon)$  is given in Eq. (B5). In solving Eq. (31),  $\mathcal{F}_{\bar{\nu}}$  must be evolved simultaneously with  $\mathcal{F}_\nu$ . To do so, in addition to making the appropriate changes to the vector and axial-vector coupling constants,  $V$  and  $A$ , one needs to integrate over  $\varepsilon_\nu$  instead of  $\varepsilon_{\bar{\nu}}$ . Note that the electron and positron distribution functions appear explicitly in Eq. (31). We take these distributions to be Fermi-Dirac at temperature  $T$  and with  $\eta_e$  determined by  $T$ ,  $\rho$ , and  $Y_e$ .

Equation (27) may also be used to find the total volumetric  $\nu_\mu \bar{\nu}_\mu$  pair spectrum by replacing  $\varepsilon_\nu$  in the numerator with  $\epsilon$ . Ignoring neutrino blocking in the final state one can show that [20]

$$Q_{\nu_{\mu}\bar{\nu}_{\mu}} \approx 2.09 \times 10^{24} \left( \frac{T}{\text{MeV}} \right)^9 f(\eta_e) \text{ ergs cm}^{-3} \text{ s}^{-1}, \quad (32)$$

where

$$f(\eta_e) = \frac{F_4(\eta_e)F_3(-\eta_e) + F_4(-\eta_e)F_3(\eta_e)}{2F_4(0)F_3(0)} \quad (33)$$

and

$$F_n(y) = \int_0^{\infty} \frac{x^n}{e^{x-y} + 1} dx \quad (34)$$

are the Fermi integrals.

#### D. Nucleon-nucleon bremsstrahlung

The importance of nucleon-nucleon bremsstrahlung in late-time neutron star cooling has been acknowledged for some time [13,14]. Recently, however, this process has received more attention as a contributor of  $\nu_{\mu}\bar{\nu}_{\mu}$  pairs and as an energy transport mechanism in both core-collapse supernova and nascent neutron star evolution [7,12,21,22]. The contribution from nucleon-nucleon bremsstrahlung is a composite of neutron-neutron (nn), proton-proton (pp), and neutron-proton (np) bremsstrahlung. Fermi's Golden Rule for the total volumetric emissivity of single  $\nu_{\mu}$ 's due to nn, pp, or np bremsstrahlung, including  $\nu_{\mu}$  and  $\bar{\nu}_{\mu}$  blocking in the final state, is given by

$$Q = \int \left[ \prod_{i=1}^4 \frac{d^3 \vec{p}_i}{(2\pi)^3} \right] \frac{d^3 \vec{q}_\nu}{(2\pi)^3 2\epsilon_\nu} \frac{d^3 \vec{q}_{\bar{\nu}}}{(2\pi)^3 2\epsilon_{\bar{\nu}}} \epsilon_\nu \left( s \sum |\mathcal{M}|^2 \right) \times (2\pi)^4 \delta^4(P) \Xi[\mathcal{F}], \quad (35)$$

where

$$\Xi[\mathcal{F}] = \mathcal{F}_1 \mathcal{F}_2 (1 - \mathcal{F}_3) (1 - \mathcal{F}_4) (1 - \mathcal{F}_\nu) (1 - \mathcal{F}_{\bar{\nu}}). \quad (36)$$

The product of differential phase space factors in Eq. (35) includes a term for each of the four nucleons involved in the process; 1 and 2 denote initial-state nucleons, whereas 3 and 4 denote final-state nucleons. In Eq. (35),  $s$  is a symmetry factor for identical initial-state fermions,  $\vec{q}_\nu$  is the neutrino three-momentum,  $\epsilon_\nu$  is the neutrino energy, and the four-momentum conserving delta function is explicit. In a one-pion exchange model for the nucleon-nucleon interaction, the spin-summed matrix element can be approximated by [13,21]

$$\sum_s |\mathcal{M}|^2 \approx 64 G^2 g_A^2 \left( \frac{f}{m_\pi} \right)^4 \left[ \left( \frac{k^2}{k^2 + m_\pi^2} \right)^2 + \dots \right] \times \epsilon^{-2} (\epsilon_\nu \epsilon_{\bar{\nu}} - \vec{q}_\nu \cdot \hat{k} \vec{q}_{\bar{\nu}} \cdot \hat{k}), \quad (37)$$

where  $\epsilon = \epsilon_\nu + \epsilon_{\bar{\nu}}$ ,  $k$  is the magnitude of the nucleon momentum transfer,  $g_A \approx -1.26$ ,  $f \sim 1$  is the pion-nucleon coupling, and  $m_\pi$  is the mass of the pion. In order to make the 18-dimensional phase-space integration in Eq. (35) tractable

we assume the quantity in square brackets to be of order unity, but possibly as low as 0.1 [12]. To acknowledge our ignorance, we introduce the factor  $\zeta$ , and assume these momentum terms are constant. Furthermore, we neglect the momentum of the neutrinos relative to the momentum of the nucleons. We are left with a simple, but general, form for the bremsstrahlung matrix element

$$\sum |\mathcal{M}|^2 \approx A \zeta \frac{\epsilon_\nu \epsilon_{\bar{\nu}}}{\epsilon^2}, \quad (38)$$

where  $A = 64 G^2 g_A^2 f^4 / m_\pi^4$ . In the case of nn or pp bremsstrahlung, as appropriate for identical particles in the initial state, the symmetry factor ( $s$ ) in Eq. (35) is 1/4. Such a symmetry factor does not enter for the mixed-nucleon process np, which is still further enhanced by the fact that a charged pion mediates the nucleon exchange [21]. This increases the matrix element in Eq. (38) by a factor of 7/3 in the degenerate nucleon limit and  $\sim 5/2$  in the nondegenerate limit [21]. Considering the already substantial simplifications made by choosing not to handle the momentum terms directly, we will adopt the more conservative  $4 \times (7/3)$  enhancement for the np matrix element. The total volumetric emission rate combining all processes is just  $Q_{\text{tot}} = Q_{\text{nn}} + Q_{\text{pp}} + Q_{\text{np}}$ . What remains is to reduce Eq. (35) to a useful expression in asymmetric matter and at arbitrary neutron and proton degeneracy.

Following Ref. [21], we define new momenta,  $p_\pm = (p_1 \pm p_2)/2$  and  $p_{3c,4c} = p_{3,4} - p_+$ , new direction cosines  $\gamma_1 = p_+ \cdot p_- / |p_+| |p_-|$  and  $\gamma_c = p_+ \cdot p_{3c} / |p_+| |p_{3c}|$ , and let  $u_i = p_i^2 / 2 mT$ . Furthermore, we note that  $d^3 p_1 d^3 p_2 = 8 d^3 p_+ d^3 p_-$ . Using the three-momentum conserving delta function, we can do the  $d^3 \vec{p}_4$  integral trivially. Rewriting Eq. (35) with these definitions, we find that

$$Q = 2 A s \zeta (2 \text{ mT})^{9/2} (2\pi)^{-9} \times \int d\epsilon_\nu \epsilon_\nu^3 \int d\epsilon_{\bar{\nu}} du_- du_+ du_{3c} d\gamma_1 d\gamma_c (\epsilon_{\bar{\nu}} / \epsilon)^2 \times (u_- u_+ u_{3c})^{1/2} \delta(E) \Xi[\mathcal{F}], \quad (39)$$

where

$$\delta(E) = \delta \left( \sum_{i=1}^4 \epsilon_i - \epsilon \right) = \delta(2T(u_- - u_{3c} - \epsilon/2T)). \quad (40)$$

The nucleon distribution functions in the term  $\Xi[\mathcal{F}]$  in Eq. (39) have been rewritten in terms of the new direction cosines, the dimensionless momenta ( $u_i$ ), and the initial-state nucleon degeneracy factors  $\eta_{1,2} = \mu_{1,2}/T$

$$\mathcal{F}_1 = \frac{e^{-(a'_1 + b' \gamma_1)}}{2 \cosh(a'_1 + b' \gamma_1)},$$

and

$$\mathcal{F}_2 = \frac{e^{-(a'_2 - b' \gamma_1)}}{2 \cosh(a'_2 - b' \gamma_1)}, \quad (41)$$

where  $a'_{1,2} = a_{1,2}/2 = \frac{1}{2}(u_+ + u_- - \eta_{1,2})$  and  $b' = b/2 = (u_+ u_-)^{1/2}$ . Furthermore,

$$(1 - \mathcal{F}_3) = \frac{e^{(c'_1 + d' \gamma_c)}}{2 \cosh(c'_1 + d' \gamma_c)}$$

and

$$(1 - \mathcal{F}_4) = \frac{e^{(c'_2 - d' \gamma_c)}}{2 \cosh(c'_2 - d' \gamma_c)}, \quad (42)$$

where  $c'_{1,2} = c_{1,2}/2 = \frac{1}{2}(u_+ + u_{3c} - \eta_{1,2})$  and  $d' = d/2 = (u_+ u_{3c})^{1/2}$ .  $\mathcal{F}_\nu$  and  $\mathcal{F}_{\bar{\nu}}$ , in contrast with the nucleon distribution functions, are independent of angle; for a given set of thermodynamic conditions, they remain functions of energy alone. While nontrivial, the integrations over  $\gamma_1$  and  $\gamma_c$  can be performed. For example, the result for the  $\gamma_1$  integration is of the form

$$\frac{1}{2\sqrt{B(B+1)}} \ln[(B - (1+2B)\xi^2 + 2\xi\sqrt{B(B+1)}(\xi^2 - 1))], \quad (43)$$

where  $B = \sinh^2 a'$  and  $\xi = \cosh b' \gamma_1$ . With a proper evaluation of the integration limits and some algebra one can rewrite this result as

$$\frac{1}{2 \sinh a' \cosh a'} \ln \left[ \frac{(1 + \cosh a \cosh b + \sinh a \sinh b)}{(1 + \cosh a \cosh b - \sinh a \sinh b)} \right]. \quad (44)$$

Similar operations yield a result for the  $\gamma_c$  integral in terms of  $c$  and  $d$ . In addition, Eq. (40) can be used to eliminate the integral over  $u_-$ . Collectively, these manipulations reveal that the differential  $\nu_\mu$  bremsstrahlung emissivity at arbitrary neutron and proton degeneracy is simply a three-dimensional integral over  $u_+$ ,  $u_{3c}$ , and  $\varepsilon_{\bar{\nu}}$

$$\begin{aligned} \frac{dQ}{d\varepsilon_\nu} &= K s \zeta (1 - \mathcal{F}_\nu) \varepsilon_\nu^3 \int d\varepsilon_{\bar{\nu}} du_+ du_{3c} \\ &\times (\varepsilon_{\bar{\nu}}/\epsilon)^2 u_+^{-1/2} e^{-\beta\epsilon/2} \Phi(\epsilon, u_+, u_{3c}) (1 - \mathcal{F}_{\bar{\nu}}), \end{aligned} \quad (45)$$

where

$$K = 2G^2 \left( \frac{m}{2\pi^2} \right)^{9/2} \left( \frac{f}{m_\pi} \right)^4 g_A^2 T^{7/2}, \quad (46)$$

$$\begin{aligned} \Phi(\epsilon, u_+, u_{3c}) &= \sinh^{-1}(f) \ln \left[ \frac{(1 + \cosh(e_+))}{(1 + \cosh(e_-))} \right] \\ &\times \left( \frac{\cosh(f) + \cosh(g_+)}{\cosh(f) + \cosh(g_-)} \right) \sinh^{-1}(j) \\ &\times \ln \left[ \frac{(1 + \cosh(h_+))}{(1 + \cosh(h_-))} \right] \\ &\times \left( \frac{\cosh(j) + \cosh(k_+)}{\cosh(j) + \cosh(k_-)} \right), \end{aligned} \quad (47)$$

and

$$\begin{aligned} e_\pm &= (u_+^{1/2} \pm u_-^{1/2})^2 - \eta_2, \\ f &= u_+ + u_- - \eta_1/2 - \eta_2/2, \\ g_\pm &= \pm 2(u_+ u_-)^{1/2} - \eta_1/2 + \eta_2/2, \\ h_\pm &= (u_+^{1/2} \pm u_{3c}^{1/2})^2 - \eta_2, \\ j &= u_+ + u_{3c} - \eta_1/2 - \eta_2/2, \\ k_\pm &= \pm 2(u_+ u_{3c})^{1/2} - \eta_1/2 + \eta_2/2. \end{aligned} \quad (48)$$

Though  $u_-$  has been integrated out via the energy-conserving delta function, it appears here in an attempt to make this expression more compact and should be read as  $u_- = u_{3c} + \epsilon/2T$ . Importantly, if  $\eta_1 = \eta_2$  the right-hand term within both logarithmic terms in  $\Phi(\epsilon, u_+, u_{3c})$  becomes unity.

Using Eq. (30), we can easily obtain the contribution to the Boltzmann equation due to nucleon-nucleon bremsstrahlung for arbitrary nucleon degeneracy, in asymmetric matter, and including the full nucleon and neutrino Pauli blocking terms. We find that

$$\begin{aligned} j_\nu &= K' s \zeta \int d\varepsilon_{\bar{\nu}} du_+ du_{3c} (\varepsilon_{\bar{\nu}}/\epsilon)^2 u_+^{-1/2} e^{-\beta\epsilon/2} \\ &\times \Phi(\epsilon, u_+, u_{3c}) (1 - \mathcal{F}_{\bar{\nu}}), \end{aligned} \quad (49)$$

where  $K' = [(2\pi)^3/4\pi]K$ . The nucleon phase-space integrations above are identical in form for the  $\nu_\mu \bar{\nu}_\mu$  absorption process,  $\nu_\mu \bar{\nu}_\mu nn \rightarrow nn$ . In this case, then, the primed energies are now associated with nucleons 1 and 2 in the above manipulations and the incident nucleons (3 and 4) have unprimed energies. If we take the form derived above for the nucleon phase-space terms, the absorption channel  $\chi_\nu$  must then contain a factor of  $e^{\beta\epsilon}$ . In addition, the blocking term  $(1 - \mathcal{F}_{\bar{\nu}})$  becomes  $\mathcal{F}_{\bar{\nu}}$ . The Boltzmann equation for the evolution of  $\mathcal{F}_\nu$  in time is then

$$\begin{aligned} \frac{\partial \mathcal{F}_\nu}{\partial t} &= K' s \zeta \int d\varepsilon_{\bar{\nu}} du_+ du_{3c} (\varepsilon_{\bar{\nu}}/\epsilon)^2 u_+^{-1/2} e^{-\beta\epsilon/2} \\ &\times \Phi(\epsilon, u_+, u_{3c}) \{ (1 - \mathcal{F}_\nu)(1 - \mathcal{F}_{\bar{\nu}}) - \mathcal{F}_\nu \mathcal{F}_{\bar{\nu}} e^{\beta\epsilon} \}. \end{aligned} \quad (50)$$

For the nn or pp bremsstrahlung contribution, we simply set  $s=1/4$  in Eq. (50) and use  $\eta_1=\eta_2=\eta_n$  or  $\eta_1=\eta_2=\eta_p$ , respectively. For the mixed nucleon (np) bremsstrahlung we set  $s=1$ , multiply Eq. (50) by  $7/3$ , and set  $\eta_1=\eta_n$  and  $\eta_2=\eta_p$ . While Eqs. (45) and (50) may not appear symmetric in  $\eta_1$  and  $\eta_2$  the logarithmic terms conspire to ensure that the rates for both np and pn bremsstrahlung are identical, as they should be. That is, it makes no difference whether we set  $\eta_n$  or  $\eta_p$  equal to  $\eta_1$  or  $\eta_2$ .

Just as in Sec. III C, in considering  $e^+e^- \leftrightarrow \nu_\mu \bar{\nu}_\mu$ ,  $\mathcal{F}_\nu^-$  must be evolved simultaneously with  $\mathcal{F}_\nu$ . In this case, however, the situation is simpler. Suppose we wish to compare electron-positron annihilation with nucleon-nucleon bremsstrahlung by starting at  $t=0$  with  $\mathcal{F}_\nu^-=\mathcal{F}_\nu=0$  over all energies. We then solve Eq. (31) and its  $\mathcal{F}_\nu^-$  counterpart at each time step and at each energy. For  $e^+e^-$  annihilation,  $\mathcal{F}_\nu$  and  $\mathcal{F}_\nu^-$  will evolve differently; they will be visibly different at each time step, because of the weighting of the vector and axial-vector coupling constants that appear in the matrix element. In contrast, Eq. (50) for bremsstrahlung must be solved only once. Since there is no difference in weighting between  $\nu_\mu$  and  $\bar{\nu}_\mu$ , we can set  $\mathcal{F}_\nu^-=\mathcal{F}_\nu$  at every energy, at every time step, as long as  $\mathcal{F}_\nu^-=\mathcal{F}_\nu$  at  $t=0$ . Of course, if we wish to consider  $\mathcal{F}_\nu^-\neq\mathcal{F}_\nu$  initially, the two distributions would need to be evolved separately and simultaneously, coupled through the blocking and source terms on the right-hand side of the Boltzmann equation.

Equation (35) can also be used to find the total volumetric  $\nu_\mu \bar{\nu}_\mu$  pair emissivity. To facilitate this we replace  $\varepsilon_\nu$  with  $\epsilon$  and insert  $\int \delta(\epsilon - (\varepsilon_\nu + \varepsilon_{\bar{\nu}})) d\epsilon$ . Assuming the neutrinos are radiated isotropically, we can use this delta function to do the integral over  $d^3\vec{q}_\nu$  and leave the total rate in terms of an integral over  $\varepsilon_\nu$  from zero to  $\epsilon$  and another over  $\epsilon$  from zero to infinity. Momentarily ignoring neutrino blocking in the final state, the former can be integrated easily. Making the same momentum, angle, and nucleon distribution function substitutions we used in deriving the single  $\nu_\mu$  spectrum we can reduce the pair spectrum to an integral over  $u_+$ ,  $u_{3c}$ , and  $q = \epsilon/2T$ . We find that

$$Q_{\nu_\mu \bar{\nu}_\mu} = D s \zeta T^{8.5} \int dq du_{3c} du_+ q^4 e^{-q} u_+^{-1/2} \Phi(\epsilon, u_+, u_{3c}), \quad (51)$$

where

$$D = \frac{8}{15} \frac{G^2 g_A^2}{\sqrt{2} \pi^9} \left( \frac{f}{m_\pi} \right)^4 m^{9/2}, \quad (52)$$

and  $\Phi(\epsilon, u_+, u_{3c})$  is defined in Eq. (47). Note that Eq. (51) allows us to easily calculate the pair differential volumetric emissivity ( $dQ_{\nu_\mu \bar{\nu}_\mu}/d\epsilon$ ). For  $Q_{\nu_\mu \bar{\nu}_\mu}^{\text{nn}}$  and  $Q_{\nu_\mu \bar{\nu}_\mu}^{\text{pp}}$ ,  $s=1/4$ . As with the single  $\nu_\mu$  spectrum, for  $Q_{\nu_\mu \bar{\nu}_\mu}^{\text{np}}$  multiply Eq. (51) by  $7/3$  and set  $s=1$ . Finally,  $Q_{\nu_\mu \bar{\nu}_\mu}^{\text{tot}} = Q_{\nu_\mu \bar{\nu}_\mu}^{\text{nn}} + Q_{\nu_\mu \bar{\nu}_\mu}^{\text{pp}} + Q_{\nu_\mu \bar{\nu}_\mu}^{\text{np}}$ .

### 1. The nondegenerate nucleon limit

In the nondegenerate nucleon limit, the term  $\mathcal{F}_1 \mathcal{F}_2 (1 - \mathcal{F}_3)(1 - \mathcal{F}_4)$  reduces to  $e^{\eta_1} e^{\eta_2} e^{-2(u_+ + u_-)}$  [12] which is independent of angle. This tremendous simplification allows for easy integration over  $u_+$  and  $u_{3c}$  in Eqs. (45), (50), and (51). The total volumetric emissivity of a single  $\nu_\mu \bar{\nu}_\mu$  pair in this limit, ignoring  $\nu_\mu$  and  $\bar{\nu}_\mu$  blocking in the final state, is [12]

$$Q_{\nu_\mu \bar{\nu}_\mu} \approx 1.04 \times 10^{30} \zeta (X \rho_{14})^2 \left( \frac{T}{\text{MeV}} \right)^{5.5} \text{ ergs cm}^{-3} \text{ s}^{-1}. \quad (53)$$

For nn and pp bremsstrahlung,  $X$  is the number fraction of neutrons  $X_n$  or protons  $X_p$ , respectively. For the mixed-nucleon process (np),  $X^2$  becomes  $(28/3)X_n X_p$ . Figure 1 compares the nondegenerate nucleon limit [Eq. (53)] with the arbitrary nucleon degeneracy generalization [Eq. (51)] in the case of nn bremsstrahlung, as a function of the neutron degeneracy  $\eta_n = \mu_n/T$ . The filled square shows the degenerate limit obtained by Ref. [14]. Note that at  $\eta_n \approx 0$ , the fractional difference between the two is just  $\sim 12\%$ . At realistic neutron degeneracies within the core ( $\eta_n \sim 2$ ), this difference approaches 30%.

The single differential  $\nu_\mu$  emissivity can be written in terms of the pair emissivity [12]

$$\begin{aligned} \frac{dQ}{d\varepsilon_\nu} &= C \left( \frac{Q_{\nu_\mu \bar{\nu}_\mu}}{T^4} \right) \varepsilon_\nu^3 \int_1^\infty \frac{e^{-2q_\nu x}}{x^3} (x^2 - x)^{1/2} dx \\ &= C \left( \frac{Q_{\nu_\mu \bar{\nu}_\mu}}{T^4} \right) \varepsilon_\nu^3 \int_{q_\nu}^\infty \frac{e^{-q}}{q} K_1(q) (q - q_\nu)^2 dq, \end{aligned} \quad (54)$$

where  $C = 2310/2048 \approx 1.128$ ,  $q_\nu = \varepsilon_\nu/2T$ ,  $q = \epsilon/2T$ , and  $K_1$  is the standard modified Bessel function of imaginary argument. A useful fit to Eq. (54), good to better than 3% over the full range of relevant neutrino energies, is [12]

$$\frac{dQ}{d\varepsilon_\nu} \sim 0.234 \frac{Q_{\nu_\mu \bar{\nu}_\mu}}{T} \left( \frac{\varepsilon_\nu}{T} \right)^{2.4} e^{-1.1\varepsilon_\nu/T}. \quad (55)$$

Using Eq. (30), we obtain the contribution to the Boltzmann equation including Pauli blocking of  $\nu_\mu$  and  $\bar{\nu}_\mu$  neutrinos in the final state

$$\begin{aligned} \frac{\partial \mathcal{F}_\nu}{\partial t} &= C s \zeta \int_0^\infty d\varepsilon_{\bar{\nu}} (\varepsilon_{\bar{\nu}}^2/\epsilon) K_1 \left( \frac{\beta\epsilon}{2} \right) e^{-\beta\epsilon/2} \\ &\quad \times \{ (1 - \mathcal{F}_\nu)(1 - \mathcal{F}_{\bar{\nu}}) - \mathcal{F}_\nu \mathcal{F}_{\bar{\nu}} e^{\beta\epsilon} \}, \end{aligned} \quad (56)$$

where

$$C = \frac{G^2 m^{4.5}}{\pi^{6.5}} \left( \frac{f}{m_\pi} \right)^4 g_A^2 T^{2.5} e^{\eta_1} e^{\eta_2} \approx \frac{2G^2 g_A^2}{\pi^{3.5}} \left( \frac{f}{m_\pi} \right)^4 m^{1.5} \frac{1}{T^{0.5}} n_1 n_2. \quad (57)$$

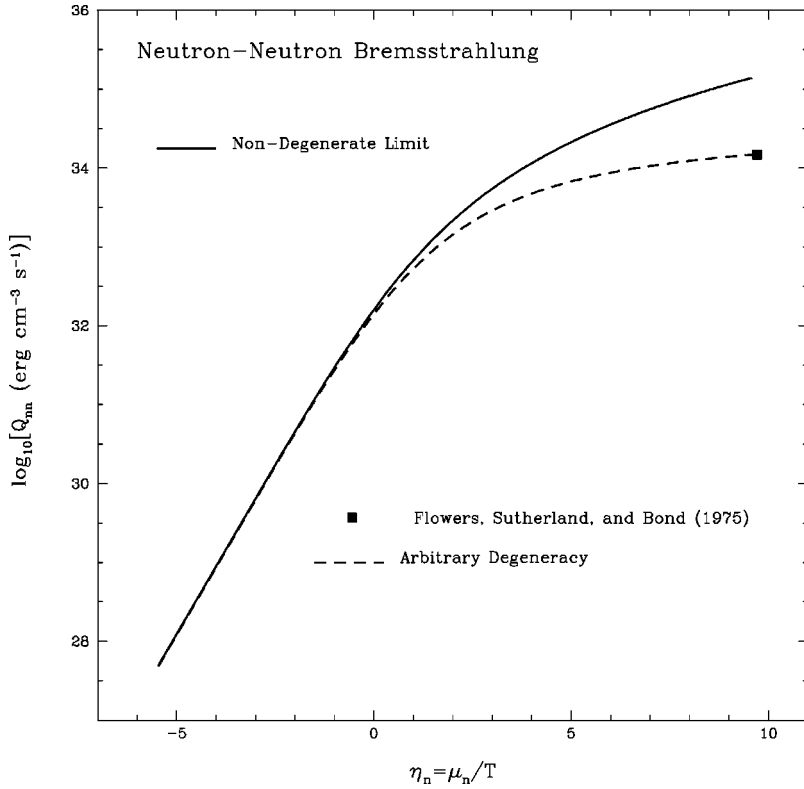


FIG. 1. The total volumetric emissivity due to neutron-neutron bremsstrahlung  $Q_{nn}$  in  $\text{ergs cm}^{-3} \text{s}^{-1}$  in the nondegenerate neutron limit [solid line, Eq. (53)] and at arbitrary nucleon degeneracy [dashed line, Eq. (51)] for  $T=6$  MeV,  $Y_e=0.0$ , and for a range of densities from  $5 \times 10^{10} \text{ g cm}^{-3}$  to nuclear density ( $\sim 2.68 \times 10^{14} \text{ g cm}^{-3}$ ). The filled box denotes the degenerate neutron limit obtained by Flowers, Sutherland, and Bond [14].

In obtaining Eq. (57), we have used the thermodynamic identity in the nondegenerate limit

$$e^{\eta_i} = \left( \frac{2\pi}{mT} \right)^{3/2} \frac{n_i}{2}, \quad (58)$$

where  $n$  is the number density of nucleons considered and  $i$  is 1 or 2 for neutrons or protons, depending on which nucleon bremsstrahlung process is considered.

#### IV. RESULTS

The numerical algorithm we have developed accepts arbitrary initial  $\nu_\mu$  and  $\bar{\nu}_\mu$  phase-space distributions. Using the scattering formalism developed in Sec. III, we evolve two initial distribution functions: (1) a broad Gaussian in energy centered at 40 MeV with a maximum of  $\mathcal{F}_\nu=0.80$  and a full width at half maximum of  $\sim 28.6$  MeV; and (2) a Fermi-Dirac distribution at a temperature two times the temperature of the surrounding matter and with zero chemical potential. While the former is unphysical in the context of supernova calculations, it illustrates the effects of blocking on both the average energy transfer and the rates for each scattering process. Furthermore, its evolution is more dynamic than the Fermi-Dirac distribution. As a result, the way in which the distribution is spread and shifted in time is more apparent. The essential differences between the two processes are then more easily gleaned. The latter initial distribution is motivated by consideration of the environment within the core of a supernova. The  $\nu_\mu$  and  $\bar{\nu}_\mu$  distribution functions, having been generated as pairs via  $e^+e^- \leftrightarrow \nu_\mu\bar{\nu}_\mu$  and nucleon-

nucleon bremsstrahlung, should have approximately zero chemical potential. Furthermore, even in the dense core, the  $\nu_\mu$ 's will diffuse outward in radius and, hence, from higher to lower temperatures. By starting with a Fermi-Dirac distribution at twice the temperature of the matter at that radius, we learn more about how equilibration might affect the emergent  $\nu_\mu$  spectrum in an actual collapse or protoneutron star cooling calculation.

For the production and absorption processes, we start with zero neutrino occupancy and let each build to an equilibrium distribution of  $\nu_\mu$ 's and  $\bar{\nu}_\mu$ 's. As a check to the calculation, the asymptotic distribution should be Fermi-Dirac at the temperature of the ambient matter with zero neutrino chemical potential. Throughout these simulations, we take the factor  $\zeta$  in Eq. (50) for nucleon-nucleon bremsstrahlung to be 0.5. (This factor represents our ignorance of the importance of the nucleon momentum transfer terms.)

We repeat these calculations for four temperature, density, and composition points (StarA, StarB, StarC, and StarD) taken from the one-dimensional collapse calculation profile, Star [3], corresponding to four radii below the shock ( $\sim 80$  km). Roughly, these points have densities  $10^{14}$ ,  $10^{13}$ ,  $10^{12}$ , and  $10^{11} \text{ g cm}^{-3}$ . The actual numbers are shown in Table I.

#### A. Scattering

Figures 2 and 3 show the evolution of a Gaussian distribution at  $t=0$  to an equilibrium Fermi-Dirac distribution at the temperature of the surrounding matter due to  $\nu_\mu$ -neutron ( $\nu_\mu n$ ) and  $\nu_\mu$ -electron ( $\nu_\mu e^-$ ) scattering, respectively. The equilibrium distribution has a nonzero neutrino chemical potential set by the initial total number of  $\nu_\mu$ 's, which is con-

TABLE I. Radius  $R$ , temperature  $T$ , density  $\rho$ , lepton fraction  $Y_e$ , and degeneracy factors  $\eta = \mu/T$  for neutrons, protons, and electrons for four points from the model, Star, a one-dimensional core-collapse calculation evolved through collapse for 0.24 s. At this point in the core evolution, the shock is at about 80 km.<sup>a</sup>

Label	$R$ (km)	$\rho$ ( $\text{g cm}^{-3}$ )	$T$ (MeV)	$Y_e$	$\eta_n$	$\eta_p$	$\eta_e$
StarA	10.75	$1.281 \times 10^{14}$	10.56	0.2752	2.37	0.70	15.75
StarB	18.75	$1.023 \times 10^{13}$	14.51	0.2021	-1.62	-3.04	3.79
StarC	34.75	$1.082 \times 10^{12}$	6.139	0.0907	-2.48	-4.81	3.03
StarD	49.75	$1.071 \times 10^{11}$	4.527	0.1671	-4.45	-6.06	1.93

<sup>a</sup>See Ref. [3].

served to better than 0.001% throughout the calculation. Multiple curves on each plot show snapshots of  $\mathcal{F}_\nu$  in time from  $t=0$  to 1000  $\mu\text{s}$ . Both calculations were carried out at the thermodynamic point StarB, whose characteristics are shown in Table I. StarB is indicative of the core of a supernova, a region of moderate to high temperatures ( $T \sim 15$  MeV) and densities of  $\sim 10^{13}$   $\text{g cm}^{-3}$ . These two figures illustrate the fundamental differences between  $\nu_\mu e^-$  and  $\nu_\mu n$  scattering as thermalization processes. Curve A in Fig. 2 and curve C in Fig. 3 indicate that at high  $\nu_\mu$  energies ( $\varepsilon_\nu \gtrsim 30$  MeV)  $\nu_\mu n$  scattering is a much more effective thermalization mechanism. At  $\varepsilon_\nu \approx 40$  MeV both curves show the distribution is within  $\sim 30\%$  of equilibrium. Importantly, however, curve A is at 0.33  $\mu\text{s}$  for  $\nu_\mu n$  scattering, whereas curve C is at 3.30  $\mu\text{s}$  for  $\nu_\mu e^-$  scattering. Curve C, in Fig. 2 for  $\nu_\mu n$  scattering, also at  $t=3.30$   $\mu\text{s}$ , shows that above  $\sim 25$  MeV the distribution has almost equilibrated. For  $\nu_\mu e^-$  scattering, similar evolution at high neutrino energies takes approximately 25  $\mu\text{s}$ . These simple estimates reveal

that  $\nu_\mu n$  scattering is about ten times faster than  $\nu_\mu e^-$  scattering at equilibrating  $\nu_\mu$ 's with energies greater than approximately 25 MeV.

This situation is reversed at low  $\varepsilon_\nu$ 's. Comparing curve E at  $t=33.0$   $\mu\text{s}$  in both Figs. 2 and 3, we can see that at  $\sim 10$  MeV both distributions have filled to approximately the same percentage of the asymptotic, equilibrium  $\mathcal{F}_\nu$ . However, below  $\varepsilon_\nu \sim 8$  MeV,  $\nu_\mu n$  scattering has not filled  $\mathcal{F}_\nu$  to the extent  $\nu_\mu e^-$  scattering has. In fact, the rate at which these low energy states are filled by  $\nu_\mu n$  scattering is very low; the energy transfer ( $\omega$ ) is much smaller than the incident  $\nu_\mu$  energy. In this regime, the Fokker-Planck approximation for the time evolution of  $\mathcal{F}_\nu$  in energy space may be applicable. In marked contrast, Fig. 3 indicates how effective  $\nu_\mu e^-$  scattering is at filling the lowest  $\varepsilon_\nu$  states. Curves F from Figs. 2 and 3, taken at 1000  $\mu\text{s}$ , show that although the distribution has reached equilibrium via  $\nu_\mu e^-$  scattering, for  $\nu_\mu n$  scattering the very lowest energy states remain unfilled. For each of the four points in the Star profile

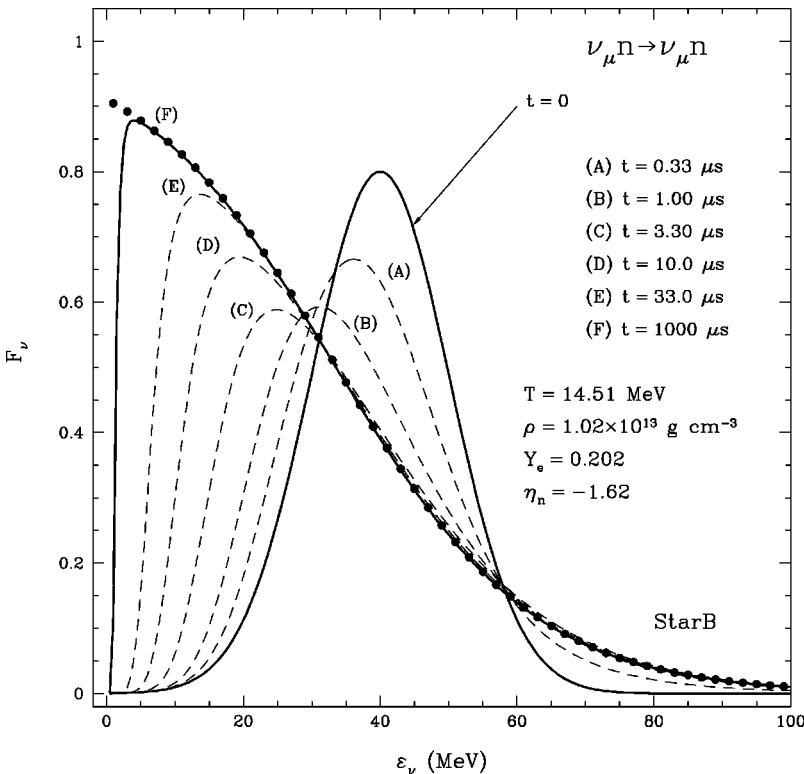


FIG. 2. The time evolution via  $\nu_\mu$ -neutron scattering of the neutrino distribution function  $\mathcal{F}_\nu$  for an initial Gaussian distribution centered on 40 MeV, for the thermodynamic characteristics specified by StarB in Table I. The curves show the distribution at snapshots in time: (A)  $t = 0.33$   $\mu\text{s}$ , (B)  $t = 1.00$   $\mu\text{s}$ , (C)  $t = 3.30$   $\mu\text{s}$ , (D)  $t = 10.0$   $\mu\text{s}$ , (E)  $t = 33.0$   $\mu\text{s}$ , and (F)  $t = 1000$   $\mu\text{s}$ . The solid dots denote an equilibrium Fermi-Dirac distribution at the temperature of the surrounding thermal bath with a neutrino chemical potential  $\mu_\nu \approx 2.32T$  set by the initial  $\nu_\mu$  neutrino number density.

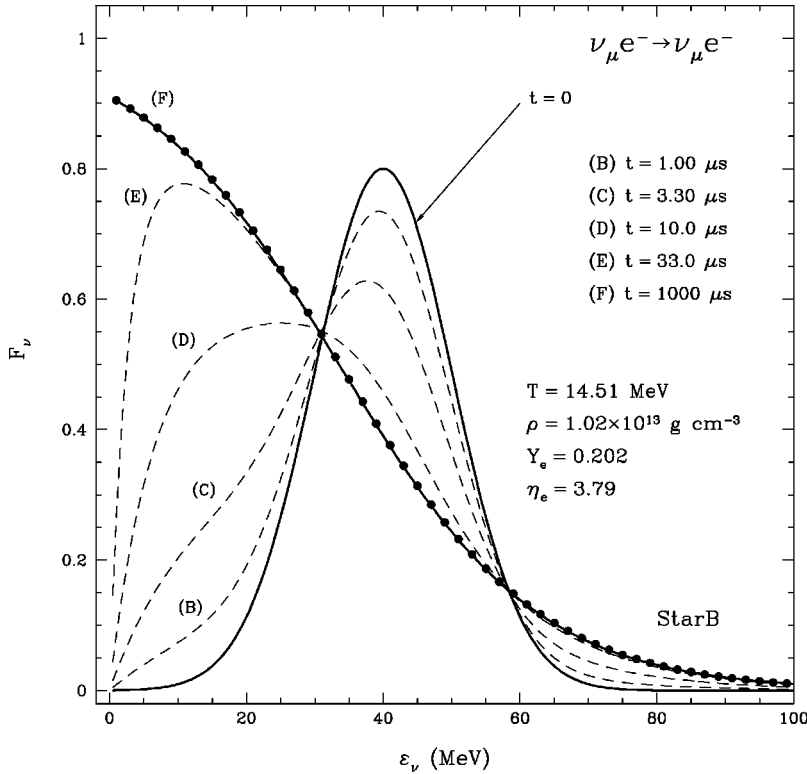


FIG. 3. The same as Fig. 2, but for  $\nu_\mu$ -electron scattering.

we consider  $\nu_\mu n$  scattering dominates at high energies ( $\geq 20$  MeV), whereas  $\nu_\mu e^-$  scattering dominates at low  $\nu_\mu$  energies ( $\leq 10$  MeV) and particularly for  $\epsilon_\nu \leq 3$  MeV.

Figures 4 and 5 depict the evolution of  $\mathcal{F}_\nu$  via  $\nu_\mu n$  and  $\nu_\mu e^-$  scattering, respectively, for an initial Fermi-Dirac dis-

tribution at two times the temperature of the surrounding neutrons and electrons and with zero neutrino chemical potential. This calculation was carried out at StarC (see Table I), which is representative of the outer core, in the semitransparent regime, where the neutrinos begin to decouple from

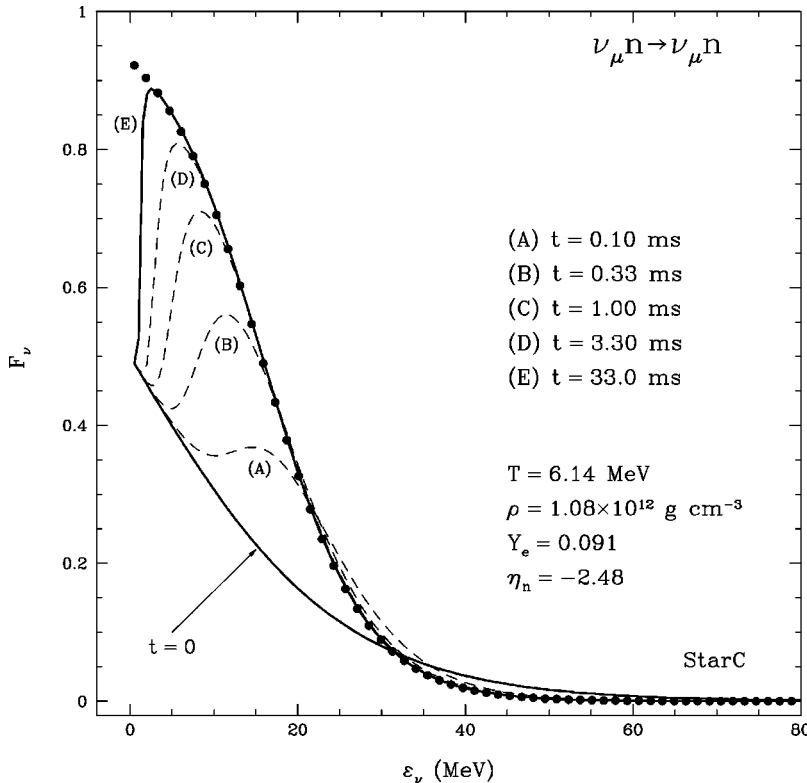


FIG. 4. The time evolution via  $\nu_\mu$ -neutron scattering of the neutrino distribution function  $\mathcal{F}_\nu$  for an initial Fermi-Dirac distribution at two times the ambient temperature, for the thermodynamic characteristics specified by StarC in Table I. The curves show the distribution at snapshots in time: (A)  $t = 0.10$  ms, (B)  $t = 0.33$  ms, (C)  $t = 1.0$  ms, (D)  $t = 3.3$  ms, and (E)  $t = 33.0$  ms. The solid dots denote an equilibrium Fermi-Dirac distribution at the temperature of the surrounding thermal bath with a neutrino chemical potential  $\mu_\nu \approx 2.55T$  set by the initial  $\nu_\mu$  neutrino number density. Comparison of this plot with Fig. 5 shows that  $\nu_\mu n$  scattering dominates thermalization above  $\epsilon_\nu \sim 10$  MeV.

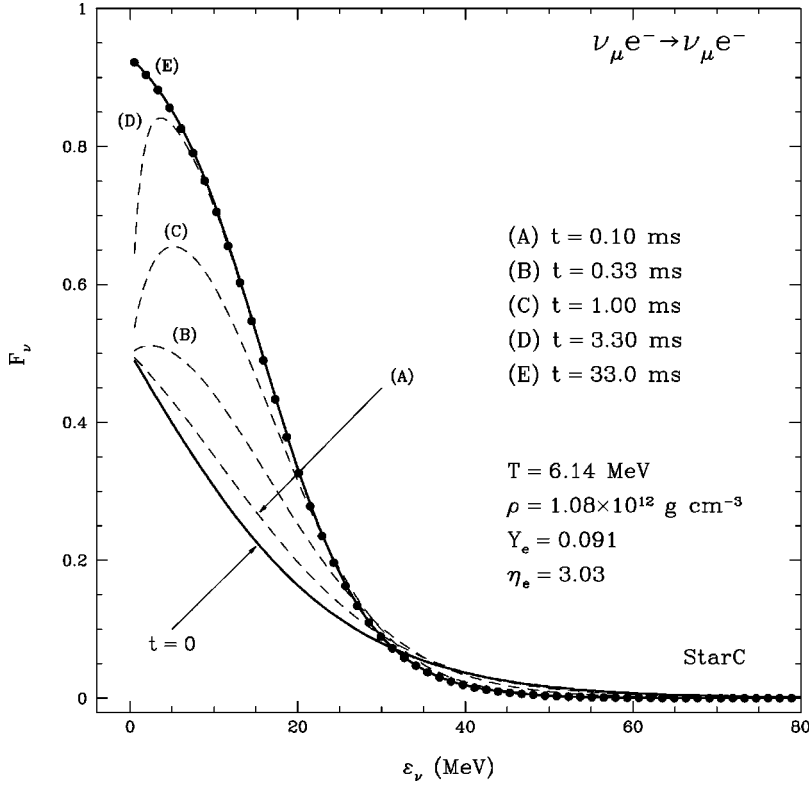


FIG. 5. The same as Fig. 4, but for  $\nu_\mu$ -electron scattering. Comparison of this plot with Fig. 4 shows that  $\nu_\mu$ -electron scattering dominates thermalization below  $\epsilon_\nu \sim 10$  MeV.

the matter (near the neutrino sphere). The same systematics highlighted in the discussion of the evolution of the initial Gaussian distribution for StarB are borne out in these figures. Curves A and B on both plots, denoting 0.10 and 0.33 ms of elapsed time, respectively, confirm that above  $\epsilon_\nu \sim 15$  MeV  $\nu_\mu n$  scattering dominates thermalization.

Figures 6 and 7 show  $\langle \omega \rangle_{\text{in}}$  and  $\langle \omega \rangle_{\text{out}}$ , as defined in Eqs. (6) and (7), for  $\nu_\mu n$  scattering and  $\nu_\mu e^-$  scattering, respectively. The separate curves portray the evolution in time of the thermal average energy transfers as the distributions evolve to equilibrium (cf. Figs. 4 and 5). As one would expect from kinematic arguments, the magnitudes of both  $\langle \omega \rangle_{\text{in}}$  and  $\langle \omega \rangle_{\text{out}}$  for  $\nu_\mu n$  scattering are much less than those for  $\nu_\mu e^-$  scattering. Although the energy transfers are much smaller, even at the highest energies,  $\nu_\mu n$  scattering still dominates  $\nu_\mu e^-$  scattering in thermalizing the  $\nu_\mu$  distribution because the rate for scattering is so much larger. At low neutrino energies, however, both average energy transfers for neutron scattering go to zero, whereas they approach large negative values ( $\sim -20$  MeV) for electron scattering. At these low energies, the fact that the rate for  $\nu_\mu n$  scattering is larger than for  $\nu_\mu e^-$  scattering fails to compensate for the vanishing energy transfer. For example, at  $\epsilon_\nu = 3$  MeV and  $t = 33$  ms, the energy transfer for  $\nu_\mu e^-$  scattering is more than 100 times that for  $\nu_\mu n$  scattering.

In order to fold in information about both the rate of scattering and the average thermal energy transfer, we plot  $\Gamma_D$  and  $\Gamma_E$  [Eqs. (8) and (9)] in Fig. 8 for all four points considered in the Star profile. We show here a snapshot of the rates for both scattering processes for a Fermi-Dirac distribution initially at twice the local matter temperature, with zero neutrino chemical potential. Note that the spikes in  $\Gamma_D$

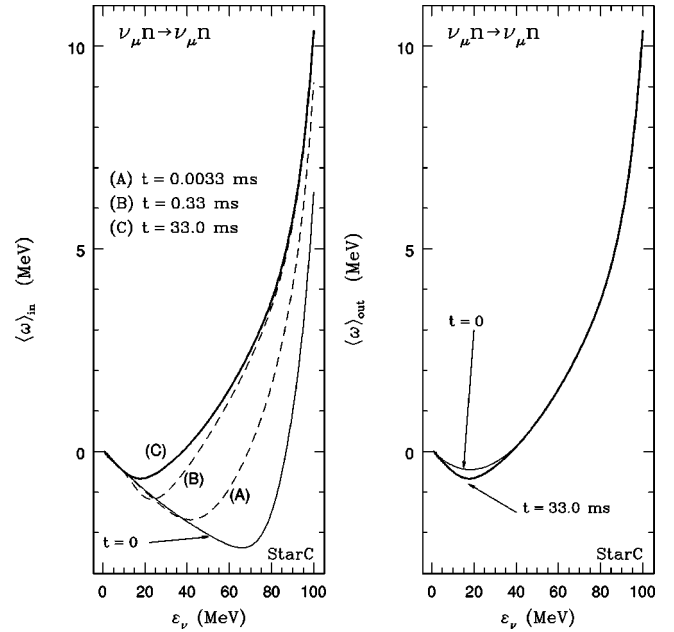


FIG. 6. The thermal average energy transfers,  $\langle \omega \rangle_{\text{in}}$  and  $\langle \omega \rangle_{\text{out}}$ , defined in Eqs. (6) and (7), respectively, as a function of neutrino energy  $\epsilon_\nu$  for  $\nu_\mu$ -neutron scattering at the thermodynamic point StarC. The curves show snapshots of the average energy transfers in time as  $\mathcal{F}_\nu$  evolves (see Fig. 4). For  $\langle \omega \rangle_{\text{in}}$ , (A)  $t = 0.0033$  ms, (B)  $t = 0.33$  ms, and (C)  $t = 33.0$  ms. We show  $\langle \omega \rangle_{\text{out}}$  at  $t = 0$  (thin line) and  $t = 33.0$  ms (thick line). Note that in equilibrium ( $t \sim 33.0$  ms)  $\langle \omega \rangle_{\text{in}} = \langle \omega \rangle_{\text{out}}$ .

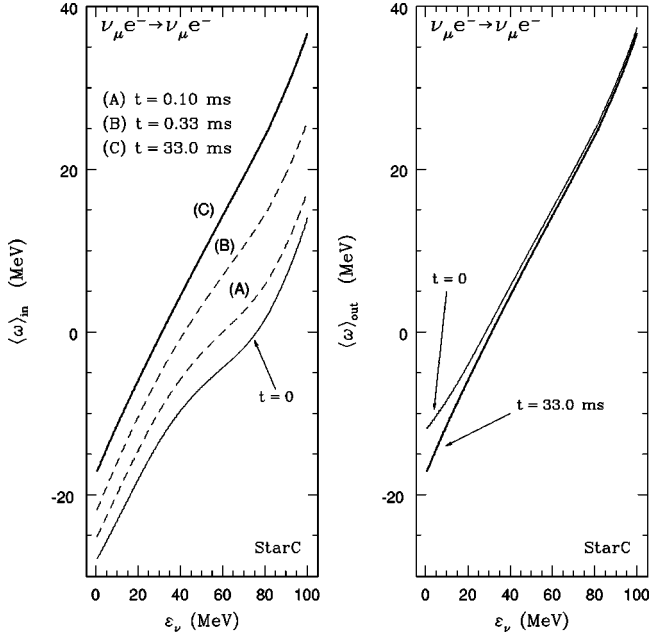


FIG. 7. The same as Fig. 6, but for  $\nu_\mu$ -electron scattering. For  $\langle \omega \rangle_{in}$ , (A)  $t = 0.10$  ms, (B)  $t = 0.33$  ms, and (C)  $t = 33.0$  ms.

indicate the neutrino energy at which  $\langle \omega \rangle_{out} = 0$  (cf. Figs. 6 and 7). In general, we find that as  $\varepsilon_\nu \rightarrow 0$ ,  $\Gamma_D$  and  $\Gamma_E$  go to zero for  $\nu_\mu$ -neutron scattering, whereas  $\Gamma_D$  approaches a constant and  $\Gamma_E$  becomes very large for  $\nu_\mu e^-$  scattering [15]. This is a consequence of the fact that, regardless of  $\mathcal{F}_\nu$ ,  $\langle \omega \rangle_{out} \rightarrow 0$  for  $\nu_\mu n$  scattering as  $\varepsilon_\nu \rightarrow 0$ , as shown in Fig. 6. For  $\nu_\mu e^-$  scattering the situation is different. As Fig. 7 reveals,  $\langle \omega \rangle_{out}$  approaches  $\sim -20$  MeV at  $\varepsilon_\nu = 0$ . As expected

from our analysis of the evolution of  $\mathcal{F}_\nu$  in Figs. 4 and 5, at approximately 40 MeV the thermalization rate for  $\nu_\mu n$  scattering for StarB is about an order of magnitude greater than that for  $\nu_\mu e^-$  scattering. Specifically, the  $\Gamma_D$ 's cross at  $\sim 15$  MeV, whereas the  $\Gamma_E$ 's cross at  $\sim 20$  MeV. Below these energies, both  $\nu_\mu n$  rates drop off precipitously as a consequence of the fact that  $\langle \omega \rangle_{out} \rightarrow 0$ . Below  $\varepsilon_\nu \sim 5$  MeV, the thermalization rate for  $\nu_\mu e^-$  scattering dominates by 2–5 orders of magnitude. As evidenced by the other panels in Fig. 8, this same trend holds in the other regions of the stellar profile. In general, the rates drop over the whole energy range for both processes as the density and temperature decrease, but the same systematics hold. In fact, for StarA, StarC, and StarD, the  $\Gamma_E$  and  $\Gamma_D$  crossing points for both processes are lower than those for StarB. As a result of the higher temperature at this radius ( $T \approx 14.5$  MeV)  $\nu_\mu e^-$  scattering is important in thermalizing slightly higher energy neutrinos than at the other radii. For StarC and StarD, specifically, both rates cross at neutrino energies less than 12 MeV.

These results demonstrate that  $\nu_\mu$ -nucleon scattering is an important thermalization process from the dense core through the semitransparent regime for  $\nu_\mu$ 's with energies greater than approximately 15 MeV. The addition of this energy transfer mechanism implies that the  $\nu_\mu$ 's stay energetically coupled to the surrounding matter longer than has been previously estimated [23]. We can approximate the radius at which the  $\nu_\mu$ 's energetically decouple from the matter (the  $E_\mu$  sphere) [23] by observing when the diffusion time scale is approximately equal to the equilibration time scale given by  $\Gamma_D^{-1} = \tau_D$ , as defined in Eq. (8). Using this crude approximation we find that by including  $\nu_\mu$ -nucleon

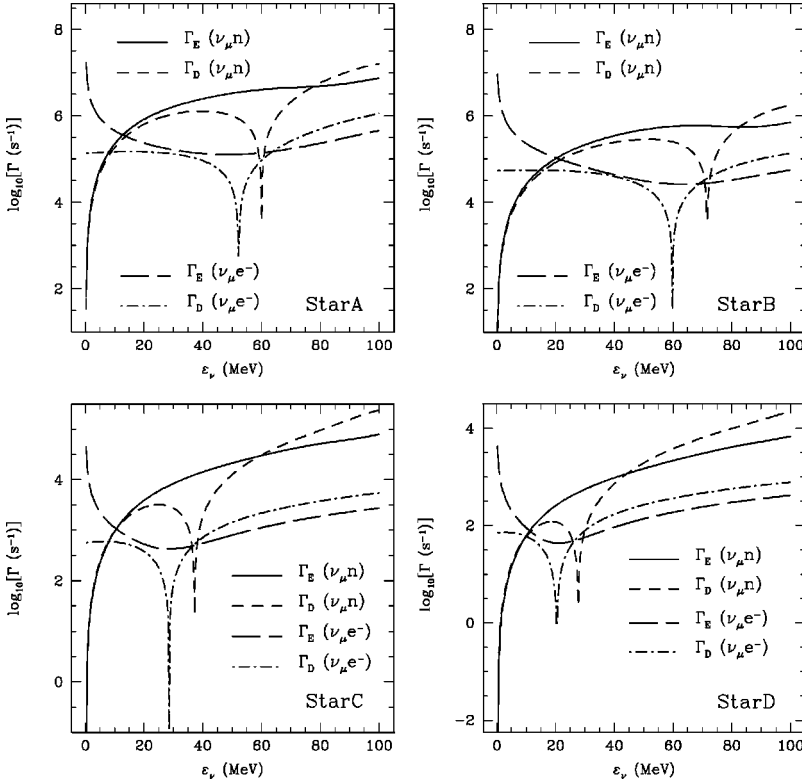


FIG. 8.  $\Gamma_D$  and  $\Gamma_E$  as defined in Eqs. (8) and (9), respectively, for both  $\nu_\mu n$  and  $\nu_\mu e^-$  scattering for an initial Fermi-Dirac distribution at StarA, StarB, StarC, and StarD (see Table I) at a snapshot in time. The spikes in the  $\Gamma_D$  curves are a consequence of the fact that  $\langle \omega \rangle_{out} \rightarrow 0$  at those neutrino energies (compare the plot above for StarA with Figs. 6 and 7). The solid and the short-dashed lines in all four plots are  $\Gamma_E$  and  $\Gamma_D$ , respectively, for  $\nu_\mu n$  scattering. The long-dashed and long-short-dashed lines are  $\Gamma_E$  and  $\Gamma_D$ , respectively, for  $\nu_\mu e^-$  scattering. At all four points in the stellar profile Star,  $\nu_\mu n$  scattering dominates  $\nu_\mu e^-$  scattering at energies above 10–20 MeV by approximately an order of magnitude. For StarA, the points where the rates for  $\nu_\mu$ -electron and  $\nu_\mu$ -neutron scattering cross are at  $\sim 8$  and  $\sim 13$  MeV. For StarB, they lie higher, at  $\sim 15$  and  $\sim 20$  MeV, due predominantly to the higher temperature at that radius. For both StarC and StarD, the rates cross at between 7 and 12 MeV.

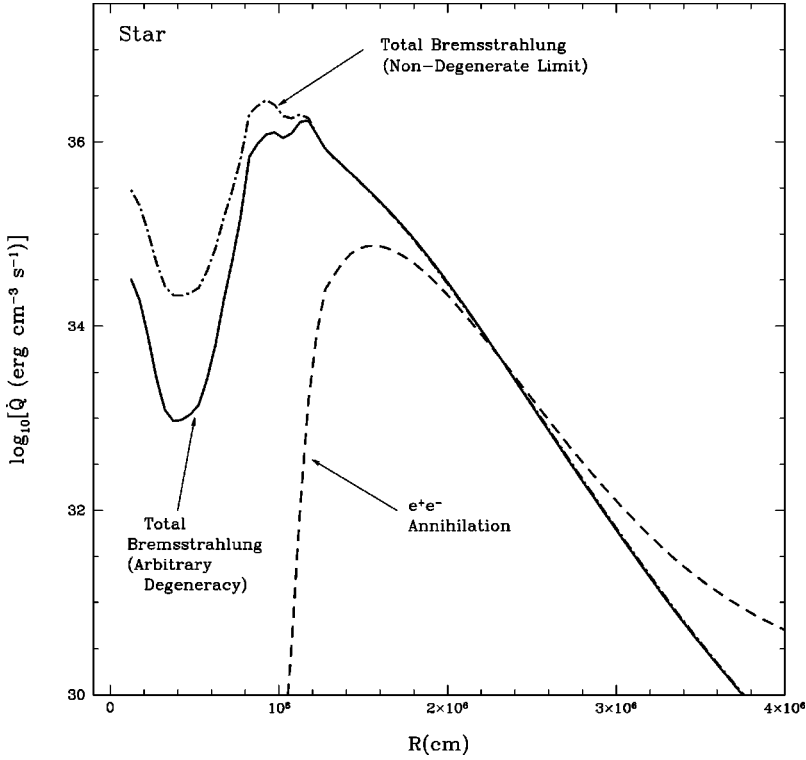


FIG. 9. The integrated total volumetric emissivity in  $\text{ergs cm}^{-3} \text{s}^{-1}$  for  $e^+e^-$  annihilation and nucleon-nucleon bremsstrahlung in the nondegenerate limit [Eq. (53)] and at arbitrary degeneracy [Eq. (45)] as a function of radius in the stellar collapse profile, Star. Note that the total bremsstrahlung and  $e^+e^-$  annihilation emissivities cross at  $R \sim 23 \text{ km}$  where  $\rho \approx 6 \times 10^{12} \text{ g cm}^{-3}$  and  $T \approx 11 \text{ MeV}$ . Above this radius,  $e^+e^-$  dominates.

energy transfer the  $E_\mu$  sphere is pushed outward in radius by approximately 3 km. This difference in radius corresponds to a 1–2 MeV drop in the matter temperature in the model Star. The average energy of the emergent spectrum is roughly correlated with the local matter temperature of the  $E_\mu$  sphere. Therefore, we conclude that  $\nu_\mu$ -nucleon energy transfer in full transport calculations will likely soften the emergent  $\nu_\mu$  spectrum.

### B. Emission and absorption

Figure 9 shows the total integrated volumetric emissivity as a function of radius in the model Star for nucleon-nucleon bremsstrahlung in the nondegenerate nucleon limit [Eq. (53)], its generalization for arbitrary nucleon degeneracy [Eq. (51)], and the emissivity for  $e^+e^-$  annihilation [Eq. (32)]. Note that not one of these expressions contains neutrino blocking terms and that the general bremsstrahlung rate crosses that for  $e^+e^-$  annihilation at  $\sim 23 \text{ km}$  where  $\rho \approx 6 \times 10^{12} \text{ g cm}^{-3}$ ,  $T \approx 11 \text{ MeV}$ , and  $Y_e \approx 0.13$ . While this plot gives a general idea of where  $e^+e^-$  annihilation should begin to compete with nucleon-nucleon bremsstrahlung, it fails to include the differential nature of the production in energy. In addition, it does not include absorption or blocking effects, which quantitatively alter the relative strength of the emission.

To begin to understand the import of these terms and the character of each pair production process, we include Figs. 10 and 11, which show the time evolution of  $\mathcal{F}_\nu$  via nucleon-nucleon bremsstrahlung and electron-positron annihilation, respectively, for the point StarC, initialized with zero  $\nu_\mu$  and  $\bar{\nu}_\mu$  phase-space occupancies. The final equilibrium distribution is Fermi-Dirac at the temperature of the surrounding

matter, with zero neutrino chemical potential. Comparing curve C on both graphs, which marks 10.0 ms of elapsed time, one can see that bremsstrahlung dominates production below  $\sim 15 \text{ MeV}$ . Indeed, bremsstrahlung overshoots its equilibrium distribution at energies below 10 MeV before finally filling the higher  $\varepsilon_\nu$  states. In contrast, electron-positron annihilation fills the higher states first and moves slowly toward the low-lying neutrino energies, taking a factor of ten more time at this thermodynamic point to reach equilibrium.

In Figs. 12 and 13, we plot  $\Gamma_{\text{in}}$  and  $\Gamma_{\text{out}}$ , as defined in Eqs. (4) and (5), for both production processes at the point StarB. As one would predict from our simple observations of the time evolution of  $\mathcal{F}_\nu$ , the bremsstrahlung rates are much faster ( $\sim 2$  orders of magnitude) than the  $e^+e^-$  annihilation rates at low neutrino energies. At StarC,  $e^+e^-$  annihilation competes with bremsstrahlung above  $\varepsilon_\nu \sim 15 \text{ MeV}$ . For StarB, however, at a matter density an order of magnitude greater than that for StarC, the energy at which nucleon-nucleon bremsstrahlung becomes more important than  $e^+e^-$  annihilation is  $\sim 60 \text{ MeV}$ . In this regime, where  $T \sim 12 - 14 \text{ MeV}$  and  $\rho \sim 10^{13} \text{ g cm}^{-3}$ , we find that bremsstrahlung dominates neutrino pair production via electron-positron annihilation. A close look at the evolution of the total thermal average neutrino energy ( $\langle \varepsilon_\nu \rangle$ ) reveals that  $\mathcal{F}_\nu$  reaches its asymptotic equilibrium distribution via nucleon-nucleon bremsstrahlung in  $\sim 1 \text{ ms}$ . Electron-positron annihilation takes  $\sim 50 \text{ ms}$  to fill all but the very lowest energy states. This trend continues as the matter becomes more dense. For StarA, well beneath the neutrinospheres at  $\rho \sim 10^{14} \text{ g cm}^{-3}$ , the rates for bremsstrahlung and electron-positron annihilation never cross. In fact, the former pro-

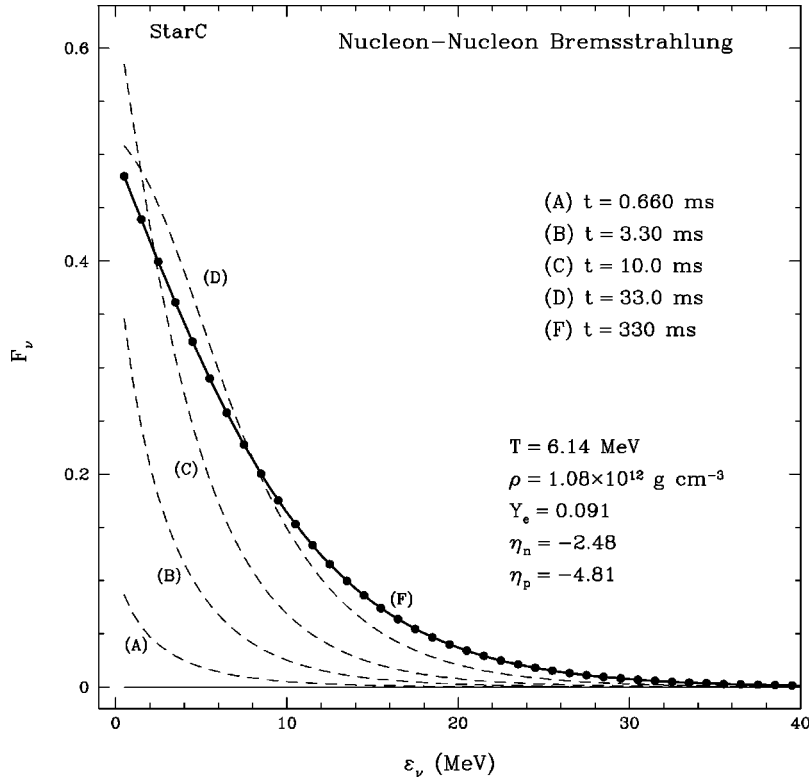


FIG. 10. The time evolution of  $\mathcal{F}_\nu$  due to nucleon-nucleon bremsstrahlung via Eq. (50) for the point StarC described in Table I starting with  $\mathcal{F}_\nu = \mathcal{F}_{\bar{\nu}} = 0$  at all energies. Curves show snapshots of the evolution of  $\mathcal{F}_\nu$  with time: (A)  $t = 0.66$  ms, (B)  $t = 3.30$  ms, (C)  $t = 10.0$  ms, (D)  $t = 33.0$  ms, and (F)  $t = 330$  ms. The solid dots denote an equilibrium Fermi-Dirac distribution at the temperature of the surrounding thermal bath with zero neutrino chemical potential.

duces an equilibrium Fermi sea of  $\nu_\mu$ 's in  $\sim 50 \mu\text{s}$ , whereas the latter takes  $\sim 10^3$  s. This difference of 8 orders of magnitude in time scale, however, is a bit misleading. Similar to  $\nu_\mu n$  scattering,  $e^+e^-$  annihilation has trouble filling only the very lowest neutrino energy states. In actuality, at the highest energies, both  $\Gamma_{\text{in}}$  and  $\Gamma_{\text{out}}$  for  $e^+e^-$  annihilation come

within 3–4 orders of magnitude of the rates for bremsstrahlung at the same energy. Still, the difference is striking. As the temperature drops from StarB (14 MeV) to StarA (10 MeV) and the density increases by an order of magnitude,  $\eta_e$  goes from 3.79 to 15.75. Consequently, Pauli blocking of electrons in the final state suppresses the process  $\nu_\mu \bar{\nu}_\mu$

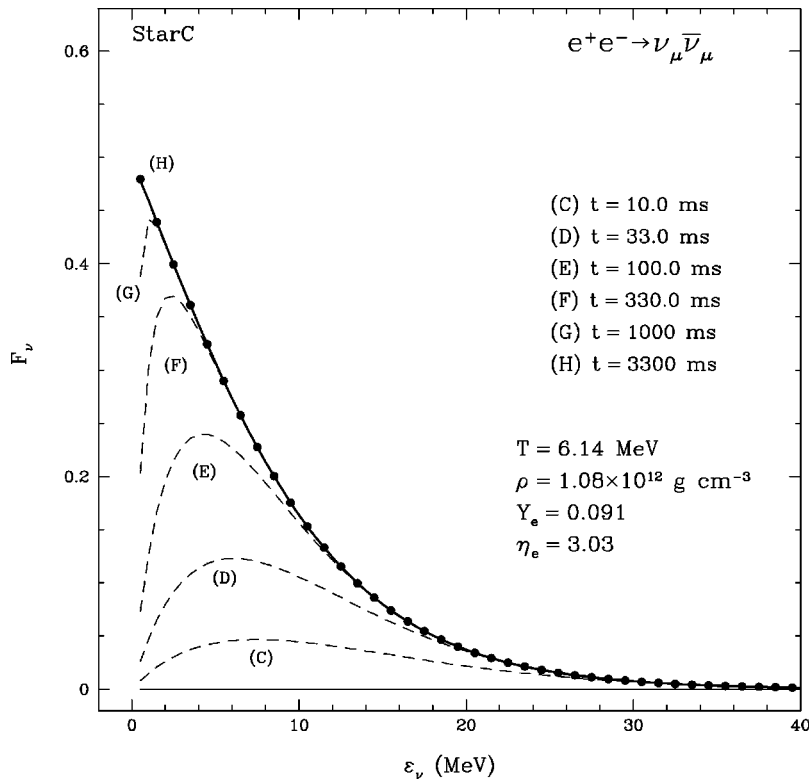


FIG. 11. The same as Fig. 10, but for  $e^+e^-$  annihilation via Eq. (31). Curves show snapshots of the evolution of  $\mathcal{F}_\nu$  with time: (C)  $t = 10.0$  ms, (D)  $t = 33.0$  ms, (E)  $t = 100.0$  ms, (F)  $t = 330.0$  ms, (G)  $t = 1000$  ms, and (H)  $t = 3300$  ms.

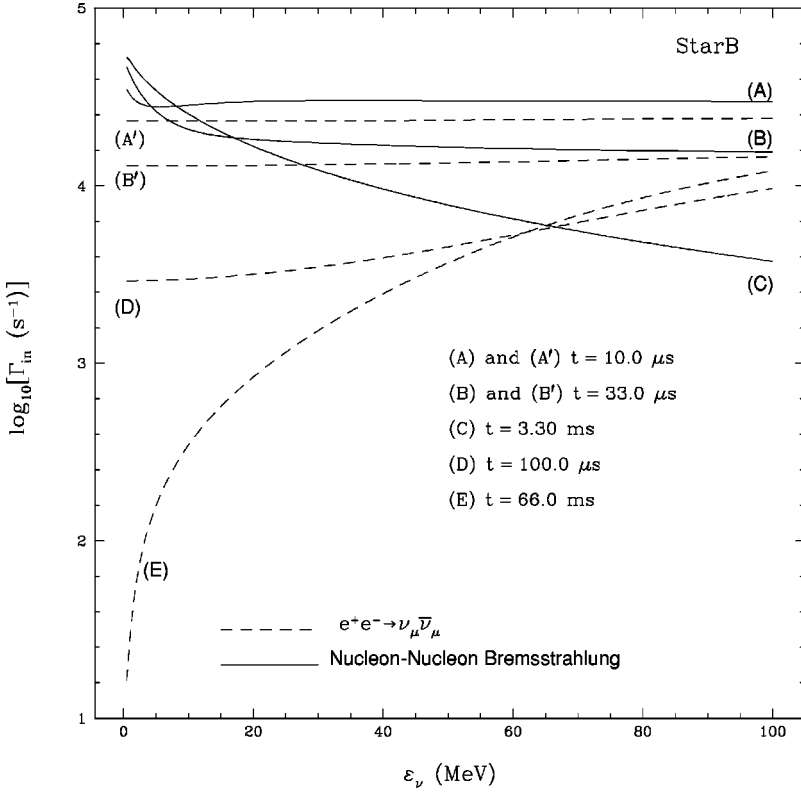


FIG. 12.  $\Gamma_{\text{in}}$  as defined in Eq. (4) for nucleon-nucleon bremsstrahlung (solid lines) and  $e^+e^-$  annihilation (dashed lines), for the point StarB. Each curve shows a snapshot of  $\Gamma_{\text{in}}$  as  $\mathcal{F}_\nu$  builds from zero phase-space occupancy at  $t=0$ : for (A) and (A')  $t=10.0 \mu\text{s}$ . (B) and (B') denote  $t=33.0 \mu\text{s}$ . (C) marks the equilibrium rate for bremsstrahlung at  $t=3.3 \text{ ms}$ . Curves (D) and (E) mark  $100.0 \mu\text{s}$  and  $66.0 \text{ ms}$ , respectively, for  $e^+e^-$  annihilation. The latter marks the  $e^+e^-$  equilibrium rate. Note that the equilibrium rates cross at  $\epsilon_\nu \sim 65 \text{ MeV}$ .

$\rightarrow e^+e^-$ , and the phase-space density of positrons is depleted to such an extent that  $e^+e^- \rightarrow \nu_\mu \bar{\nu}_\mu$  is suppressed as well. We conclude that beneath the neutrino spheres and specifically for  $\rho \sim 10^{13} \text{ g cm}^{-3}$ , nucleon-nucleon bremsstrahlung is the primary and dominant  $\nu_\mu \bar{\nu}_\mu$  source. Near the neutrino

sphere, within the gain region and behind the shock, between 30 and 60 km at  $\rho \sim 10^{12} \text{ g cm}^{-3}$  and  $T \sim 6-8 \text{ MeV}$ , bremsstrahlung competes with  $e^+e^-$  annihilation at all neutrino energies and is the primary production process for the low-lying  $\epsilon_\nu$  and  $\epsilon_{\bar{\nu}}$  states.

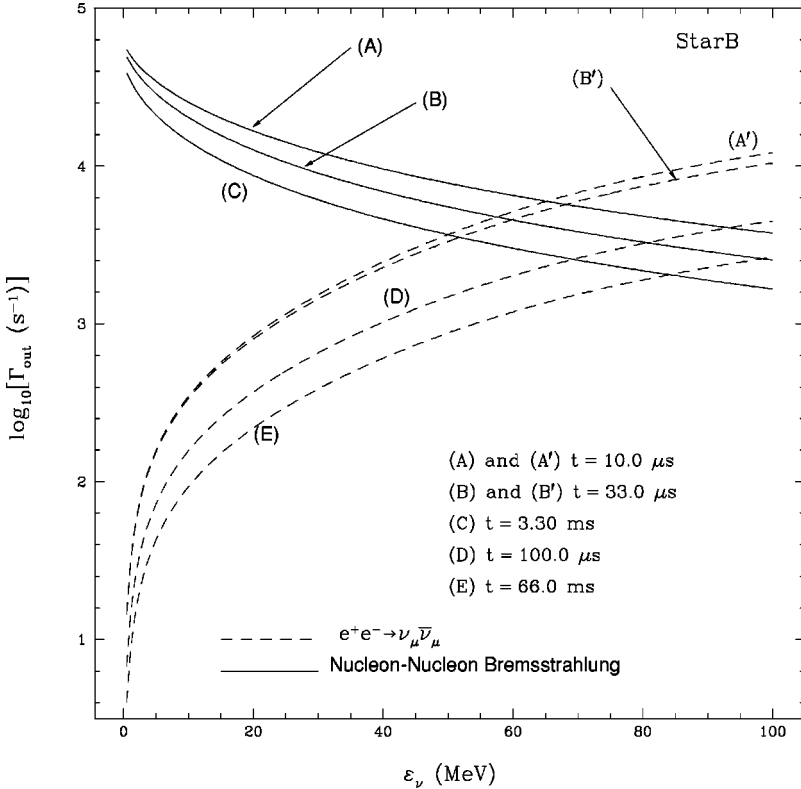


FIG. 13. The same as Fig. 12, for the same times, but for  $\Gamma_{\text{out}}$  as defined in Eq. (5).

The addition of nucleon-nucleon bremsstrahlung will have quantitative implications for the  $\nu_\mu$  and  $\nu_\tau$  emergent spectra. Specifically, they should be softer and brighter. Burrows *et al.* [12] confirm this with their study of static supernova and protoneutron star atmospheres, having included nucleon-nucleon bremsstrahlung in the nondegenerate limit. In addition to observing a systematic softening, they also find that the  $\nu_\mu$  spectrum is a factor of 2 more luminous at  $\varepsilon_\nu = 10$  MeV.

### V. SUMMARY AND CONCLUSIONS

Our results for equilibration via  $\nu_\mu$ -electron scattering and  $\nu_\mu$ -nucleon scattering indicate that the latter competes with or dominates the former as a thermalizer for neutrino energies  $\geq 10$  MeV for  $\rho \geq 1 \times 10^{11}$  g cm $^{-3}$  at all temperatures. At neutrino energies  $\geq 30$  MeV the difference at all densities and temperatures is approximately an order of magnitude. For the production and absorption processes, we find that nucleon-nucleon bremsstrahlung, at the average energy of an equilibrium Fermi-Dirac distribution at the local temperature, is 5 and 2 orders of magnitude faster than  $e^+e^-$  annihilation at StarA ( $T \sim 10$  MeV,  $\rho \sim 10^{14}$  g cm $^{-3}$ ) and StarB ( $T \sim 15$  MeV,  $\rho \sim 10^{13}$  g cm $^{-3}$ ), respectively. Only for  $\rho \sim 10^{12}$  g cm $^{-3}$  and  $T \sim 6$  MeV does  $e^+e^- \leftrightarrow \nu_\mu \bar{\nu}_\mu$  begin to compete with bremsstrahlung at all energies. We conclude from this study that the emergent  $\nu_\mu$  and  $\nu_\tau$  spectrum is (1) brighter and (2) softer than previously estimated. The former results from the inclusion of the new pair emission process, nucleon-nucleon bremsstrahlung. The latter is a consequence of both the increased energy coupling between the nuclear and neutrino fluids through  $\nu_\mu$ -nucleon scattering and the fact that bremsstrahlung dominates  $e^+e^-$  annihilation near the neutrino spheres at the lowest neutrino energies. While the full transport problem, including  $\nu_\mu$ -nucleon scattering energy redistribution and nucleon-nucleon bremsstrahlung, must be solved in order to delineate precisely what consequences these processes have for the emergent  $\nu_\mu$  spectrum, these calculations demonstrate that they should not be omitted.

### ACKNOWLEDGMENTS

The authors would like to thank Sanjay Reddy for very helpful correspondence and Georg Raffelt for a critical reading of the text. J.E.H. extends his gratitude to the Fundaç~ao de Amparo a Pesquisa do Estado de S~ao Paulo in supporting this research. This work is supported under NSF Grant No. AST96-14794.

### APPENDIX A: NEUTRINO-ELECTRON SCATTERING

Each of the retarded polarization functions in Eqs. (24)–(26) can be written in terms of one-dimensional integrals over electron energy ( $\varepsilon_e$ ), which we label  $I_n$  [4]

$$\text{Im } \Pi_L^R(q, \omega) = \frac{q_\mu^2}{2\pi|q|^3} \left[ I_2 + \omega I_1 + \frac{q_\mu^2}{4} I_0 \right], \quad (\text{A1})$$

$$\text{Im } \Pi_T^R(q, \omega) = \frac{q_\mu^2}{4\pi|q|^3} \left[ I_2 + \omega I_1 + \left( \frac{q_\mu^2}{4} + \frac{q^2}{2} + m^2 \frac{q^2}{q_\mu^2} \right) I_0 \right], \quad (\text{A2})$$

$$\text{Im } \Pi_A^R(q, \omega) = \frac{m^2}{2\pi|q|} I_0, \quad (\text{A3})$$

and

$$\text{Im } \Pi_{VA}^R(q, \omega) = \frac{q_\mu^2}{8\pi|q|^3} [\omega I_0 + 2I_1]. \quad (\text{A4})$$

The authors of Ref. [4] were able to express the  $I_n$ 's in terms of polylogarithmic integrals such that

$$I_0 = Tz \left( 1 - \frac{\xi_1}{z} \right), \quad (\text{A5})$$

$$I_1 = T^2 z \left( \eta_e - \frac{z}{2} - \frac{\xi_2}{z} - \frac{e - \xi_1}{zT} \right), \quad (\text{A6})$$

and

$$I_2 = T^3 z \left( \eta_e^2 - z\eta_e + \frac{\pi^2}{3} + \frac{z^2}{3} + 2\frac{\xi_3}{z} - 2\frac{e - \xi_2}{Tz} + \frac{e^2 - \xi_1}{T^2 z} \right), \quad (\text{A7})$$

where  $\eta_e = \mu_e/T$  is the electron degeneracy,  $z = \beta\omega$ ,  $\omega$  is the energy transfer, and

$$e_- = -\frac{\omega}{2} + \frac{q}{2} \sqrt{1 - 4\frac{m^2}{q_\mu^2}}. \quad (\text{A8})$$

In Eqs. (A5)–(A7), the  $\xi_n$ 's are differences between polylogarithmic integrals;  $\xi_n = \text{Li}_n(-\alpha_1) - \text{Li}_n(-\alpha_2)$ , where

$$\text{Li}_n(y) = \int_0^y \frac{\text{Li}_{n-1}(x)}{x} dx, \quad (\text{A9})$$

and  $\text{Li}_1(x) = \ln(1-x)$ . The arguments necessary for computing the integrals are  $\alpha_1 = \exp[\beta(e_- + \omega) - \eta_e]$  and  $\alpha_2 = \exp(\beta e_- - \eta_e)$ .

### APPENDIX B: ELECTRON-POSITRON ANNIHILATION

The production kernel is defined by

$$R^P(\varepsilon_\nu, \varepsilon_{\bar{\nu}}, \cos \theta) = \frac{1}{2\varepsilon_\nu \varepsilon_{\bar{\nu}}} \int \frac{d^3 \vec{p}}{(2\pi)^3 2\varepsilon} \frac{d^3 \vec{p}'}{(2\pi)^3 2\varepsilon'} \mathcal{F}_{e^-} \mathcal{F}_{e^+} \times \left( \frac{1}{4} \sum_s |\mathcal{M}|^2 \right) (2\pi)^4 \delta^4(P). \quad (\text{B1})$$

The differential production spectrum for final state  $\nu_\mu$ 's can then be written as [2]

$$\frac{dQ}{d\varepsilon_\nu} = (1 - \mathcal{F}_\nu) \frac{\varepsilon_\nu^3}{(2\pi)^6} \int d\Omega \int_0^\infty \varepsilon_{\bar{\nu}}^2 d\varepsilon_{\bar{\nu}} \int_{-1}^1 d\mu' \int_0^{2\pi} d\phi$$

$$\times R^p(\varepsilon_\nu, \varepsilon_{\bar{\nu}}, \cos \theta) (1 - \mathcal{F}_{\bar{\nu}}), \quad (\text{B2})$$

where  $d\Omega$  is the differential solid angle for the  $\nu_\mu$  neutrino,  $\mu' = \cos \theta'$  is the cosine of the  $\bar{\nu}_\mu$  angular coordinate, and  $\phi$  is the azimuthal angle between  $\nu_\mu$  and  $\bar{\nu}_\mu$ . Expanding the production kernel in a Legendre series in the scattering angle,  $\cos \theta = \mu\mu' + [(1 - \mu^2)(1 - \mu'^2)]^{1/2} \cos \phi$ ,

$$R^p(\varepsilon_\nu, \varepsilon_{\bar{\nu}}, \cos \theta) = \frac{1}{2} \sum_l (2l+1) \Phi_l^p(\varepsilon_\nu, \varepsilon_{\bar{\nu}}) P_l(\cos \theta)$$

$$\sim \frac{1}{2} \Phi_0^p(\varepsilon_\nu, \varepsilon_{\bar{\nu}}) + \frac{3}{2} \Phi_1^p(\varepsilon_\nu, \varepsilon_{\bar{\nu}}) \cos \theta. \quad (\text{B3})$$

$\Phi_0^p$ , in Eqs. (29) and (B3), is given by [2,24]

$$\Phi_0^p(\varepsilon_\nu, \varepsilon_{\bar{\nu}}) = \frac{G^2}{\pi} \int_0^{\varepsilon_\nu + \varepsilon_{\bar{\nu}}} d\varepsilon \mathcal{F}_{e^-} \mathcal{F}_{e^+} H_0(\varepsilon_\nu, \varepsilon_{\bar{\nu}}, \varepsilon), \quad (\text{B4})$$

where  $\mathcal{F}_{e^+}$  is a function of  $\varepsilon' (= \varepsilon_\nu + \varepsilon_{\bar{\nu}} - \varepsilon)$  and

$$H_0(\varepsilon_\nu, \varepsilon_{\bar{\nu}}, \varepsilon) = (V+A)^2 J_0^I(\varepsilon_\nu, \varepsilon_{\bar{\nu}}, \varepsilon)$$

$$+ (V-A)^2 J_0^{II}(\varepsilon_\nu, \varepsilon_{\bar{\nu}}, \varepsilon). \quad (\text{B5})$$

Each  $J_0$  in Eq. (B5) is a polynomial in  $\varepsilon_\nu$ ,  $\varepsilon_{\bar{\nu}}$ , and  $\varepsilon$  of dimension (energy). They are related to each other by [2]

$$J_0^I(\varepsilon_\nu, \varepsilon_{\bar{\nu}}, \varepsilon) = J_0^{II}(\varepsilon_{\bar{\nu}}, \varepsilon_\nu, \varepsilon). \quad (\text{B6})$$

Both  $J_0^I$  and  $J_0^{II}$  can be found in Ref. [2] [correcting for the typo in their Eq. (C67)]. From Eqs. (29) and (B5) we see that the differences between the spectra for  $\nu_\mu$ 's and  $\bar{\nu}_\mu$ 's for a given temperature and electron degeneracy  $\eta_e$  arise solely from the relative weighting constants  $(V+A)^2$  and  $(V-A)^2$  in Eq. (B5) for  $J_0^I$  and  $J_0^{II}$ , respectively. Indeed, in this approximation the same can be said for the difference in the spectrum between  $\nu_e$  and  $\nu_\mu$  neutrinos.

- 
- [1] D. Lamb and C. Pethick, *Astrophys. J. Lett.* **209**, L77 (1976).  
[2] S. Bruenn, *Astrophys. J., Suppl.* **58**, 771 (1985).  
[3] A. Burrows, J. Hayes, and B. A. Fryxell, *Astrophys. J.* **450**, 830 (1995).  
[4] S. Reddy, M. Prakash, and J. M. Lattimer, *Phys. Rev. D* **58**, 013009 (1998).  
[5] A. Burrows and R. Sawyer, *Phys. Rev. C* **58**, 554 (1998).  
[6] A. Burrows and R. Sawyer, *Phys. Rev. C* **59**, 510 (1999).  
[7] S. Hannestad and G. Raffelt, *Astrophys. J.* **507**, 339 (1998).  
[8] W. Keil, H.-T. Janka, and G. G. Raffelt, *Phys. Rev. D* **51**, 6635 (1995).  
[9] H.-T. Janka, W. Keil, G. Raffelt, and D. Seckel, *Phys. Rev. Lett.* **76**, 2621 (1996).  
[10] G. Raffelt and D. Seckel, *Phys. Rev. Lett.* **67**, 2605 (1998).  
[11] G. Sigl, *Phys. Rev. D* **56**, 3179 (1997).  
[12] A. Burrows, T. Young, P. Pinto, R. Eastman, and T. A. Thompson, *Astrophys. J.* (to be published).  
[13] B. L. Friman and O.V. Maxwell, *Astrophys. J.* **232**, 541 (1979).  
[14] E. G. Flowers, P. G. Sutherland, and J. R. Bond, *Phys. Rev. D* **12**, 315 (1975).  
[15] D. L. Tubbs, *Astrophys. J.* **231**, 846 (1979).  
[16] D. L. Tubbs, *Astrophys. J., Suppl.* **37**, 287 (1978).  
[17] D. L. Tubbs, T. A. Weaver, R. L. Bowers, J. R. Wilson, and D. N. Schramm, *Astrophys. J.* **239**, 271 (1980).  
[18] A. L. Fetter and J. D. Walecka, *Quantum Theory of Many Particle Systems* (McGraw-Hill, New York, 1971).  
[19] J. Pons, J. Miralles, and J. Ibáñez, *Astron. Astrophys., Suppl. Ser.* **129**, 343 (1998).  
[20] D. A. Dicus, *Phys. Rev. D* **6**, 941 (1975).  
[21] R. P. Brinkmann and M. S. Turner, *Phys. Rev. D* **38**, 2338 (1998).  
[22] H. Suzuki, in *Frontiers of Neutrino Astrophysics*, edited by Y. Suzuki and K. Nakamura (Universal Academy, Tokyo, 1993), p. 219.  
[23] A. Burrows and T. J. Mazurek, *Astrophys. J.* **259**, 330 (1982).  
[24] W. R. Yueh and J. R. Buchler, *Astrophys. Space Sci.* **41**, 221 (1976).